Group 2: Final Report – Aircraft Stability and Control Project

Victor Zaharia, Amir Bakhouch, Cole Schumacher, Connor Fitzpatrick,

John Munday, Mitchell Lacle, Ron Achille, Nathan Stephens.

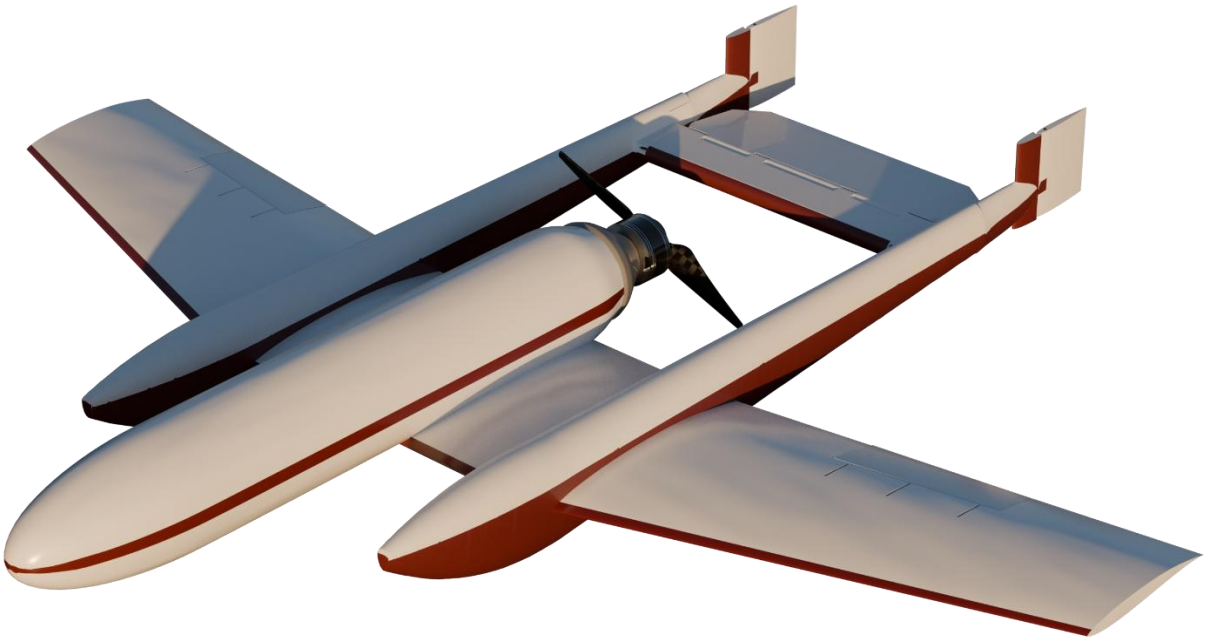

Executive Summary

Objective Statement:

The objective of this project is to design and construct an airplane capable of carrying an 8 oz Coke can payload, which will be hand-launched and must complete the highest possible number of laps in a 5-minute flyoff. The airplane's performance will be judged based on the number of completed laps, and non-conventional designs will receive additional points for creativity. The airplane must adhere to strict material and component constraints, using only the specified components listed. The goal is to maximize lap completion and incorporate innovative design elements to achieve a high overall score for the competition.

Planned Approach:

The airplane design approach will consist of using the insulation foam available at the Harris Senior Design Center (HSDC). The lightweight foam will provide the necessary structural integrity while allowing us to keep the overall weight manageable for flight. The 8 oz Coke payload will be securely mounted to the airplane, ensuring proper balance and minimal drag. The components provided such as the Brushless Direct Current Electric motor, Electronic Speed Controller (ESC), receiver, control surface motors, control horns, and wiring will be used to construct the airplane's propulsion and control systems. The airplane will be focused on maintaining stability while optimizing its flight time and lap count.

The design will include careful attention to the aerodynamic properties of the airplane, focusing on wing shape, control surface configuration, and overall flight stability. The team will integrate the supplied control surface motors and control horns to ensure responsive maneuverability. The propeller, motor, and ESC will be selected and integrated to provide efficient propulsion while supporting the weight of the payload. The battery will be chosen to ensure sufficient flight time within the 5-minute flyoff window. Epoxy will be used to primarily bond components and reinforce the structure where necessary, ensuring durability during the flight tests.

To validate the airplane's design, a series of test flights will be conducted to ensure it can carry the payload and achieve stable, sustained flight. Computer Aided Design (CAD) models will be designed, Finite Element Analysis (FEA), and Computational Fluid Dynamics (CFD) will be conducted to analyze and verify the structural integrity and aerodynamic performance of the airplane, ensuring it can withstand the forces during flight while minimizing weight and drag for maximum efficiency and stability. Based on test results, adjustments will be made to the airplane's components and design to optimize its performance. Testing will focus on increasing flight efficiency, stability, and overall lap count. The incorporation of creative design features into the airplane may include non-conventional aerodynamic modifications for enhancing overall aircraft performance.

The team will develop a flight strategy to maximize lap completion in preparation for the flyoff. With careful planning, testing, and creative design, the team is confident the airplane will meet all requirements and achieve a high score in the competition and creativity factor. The planned approach will follow the timeline provided for each milestone completion. The members of Group 2 shall dedicate time(s) to discuss elements of the project.

Management Summary

Organization

A student-organized team working along with the guidelines provided by the professor. The roles of the team will be based upon the different subsystems that will need to be developed for the entire remote control (RC) aircraft system to work and meet requirements.

The roles are divided as:[1]

- **Project Manager:** Victor Zaharia
- **Lead Systems Engineer:** Ronald Achille
- **Structures Engineer(s):** Connor Fitzpatrick, Amir Bakhouch
- **Software Engineer(s):** Mitchell Lacle, Cole Schumacher
- **Manufacturing Engineer(s):** John Munday
- **Support Engineer(s):** Nathan Stephens

The responsibility/skill set required for each role is defined as:[2]

- **Project Manager:** Oversees project and coordinates management, scheduling, and team communications.
- **Lead Systems Engineer:** Works closely with each subsystem to ensure each developed subsystem works when the project is fully assembled.
- **Structures Engineer(s):** Develops the necessary structural elements of the project.
- **Software Engineer(s):** Develops the necessary electrical elements of the project.
- **Manufacturing Engineer(s):** Tasked with developing the manufacturing plan for the full assembly of the project.
- **Support Engineer(s):** Provides assistance to each section of the project as needed.

[1] The listed roles are subject to change depending on the requirements provided by the professor.
[2] Other duties including but not limited to the design, development, and testing of the plane will be a shared responsibility of each team member.

Project Schedule

Task	W 1	W 2	W 3	W 4	W 5	W 6	W 7	W 8	W 9	W 10	W 11	W 12	W 13	W 14
Milestone 1														
Team Formation & Role Assignment														
Conceptual Design Approach														
Report Formatting & Readability Review														
Milestone 2														
Finalize Team Roles & Budget/Material Planning														
Iteration 2: Detailed Design Components														
Stability Analysis (Longitudinal & Lateral)														
Report Formatting & Readability Review														
Milestone 3														
Iteration 3/4: Design Refinement														
Finalized CAD Assembly & Stability Tests														
Report Formatting & Readability Review														

Table 1: Gannt chart displaying anticipated project timelines

Bill of Materials

Description	Cost per Unit	Qty	Cost
Transmitter	$199.00	1	$199.00
Receivers	$10.99	10	$109.99
Control Surface Motors	$19.99	4	$79.96
Propellers, motors, ESC	$22.99	10	$229.90
Control horn	$9.00	5	$45.00
Battery	$29.99	4	$119.96
Epoxy	$10.00	3	$30.00
Transmitter batteries	$25.00	2	$50.00
			Total Cost
			$863.81

Table 2: Provided Bill of Materials

The Bill of Materials has been provided by Dr. Karra and can be seen in Table 2 above.[3]

Description	Cost per Unit	Qty	Cost
Transmitter	$199.00	1	$199.00
Receivers	$10.99	1	$10.99
Control Surface Motors	$19.99	1	$19.99[4]
Propellers, motors, ESC	$22.99	1	$22.99
Control horn	$9.00	1	$9.00
Battery	$29.99	1	$29.99
Epoxy	$10.00	1	$10.00
Transmitter batteries	$25.00	1	$25.00
			Total Cost
			$326.96[5]

Table 3: Bill of Materials for Group 2

[3] https://fltech-my.sharepoint.com/:x:/g/personal/pkarra_fit_edu/EURIoaPiKg5Hm_-F89BKHHYBD5wEjJcERJO-1RykyMMuNA?rtime=8oGyUrto3Ug
[4] Each package comes in twelve.
[5] Price before tax.

Conceptual Design Approach

Mission Requirements

- Hand launched.
- Remain stable while airborne.
- Have the payload capacity to carry an 8 oz Coke can.
- Have ability to control and communicate with the aircraft while airborne.
- Must be capable of performing 360-degree turn.
- Complete as many laps as possible.

Preliminary Design

- To maximize flight score, the incorporation of non-standard elements was deemed mandatory.
- As those features can be difficult to model using standard equations, a real-life analogue was chosen to act as a jumping-off point justifying the placement and sizing of said elements.
- Preliminary model based off the Swedish SAAB 21 airplane.
- Main features consist of pusher propeller, double rudder, and swept wings.
- To accommodate the payload, a new fuselage shape and size was chosen, with the entire aircraft being resized using a series of ratios derived from aircraft blueprints to account for the modification.
- The current design is simplified but allows for modifications and adjustments, such as a compartment for the expected payload, motor mount plate, and inclusion of internal structures and wiring.
- Future alterations will be made to the plane design to account for the slower flight speed and lower altitude envelope experienced by the model airframe.

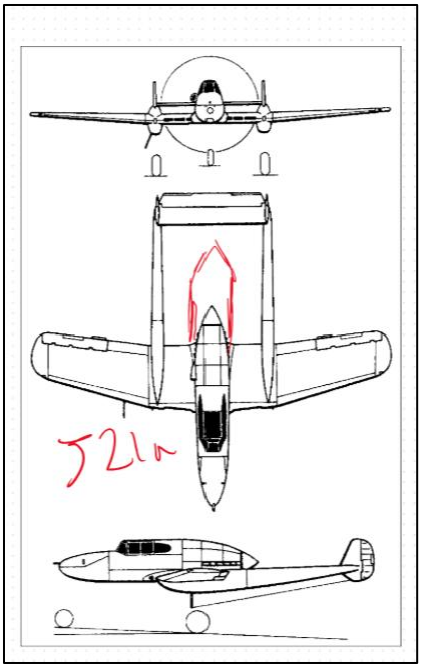

Figure 1: SAAB J21a with proposed modification (shown in red)

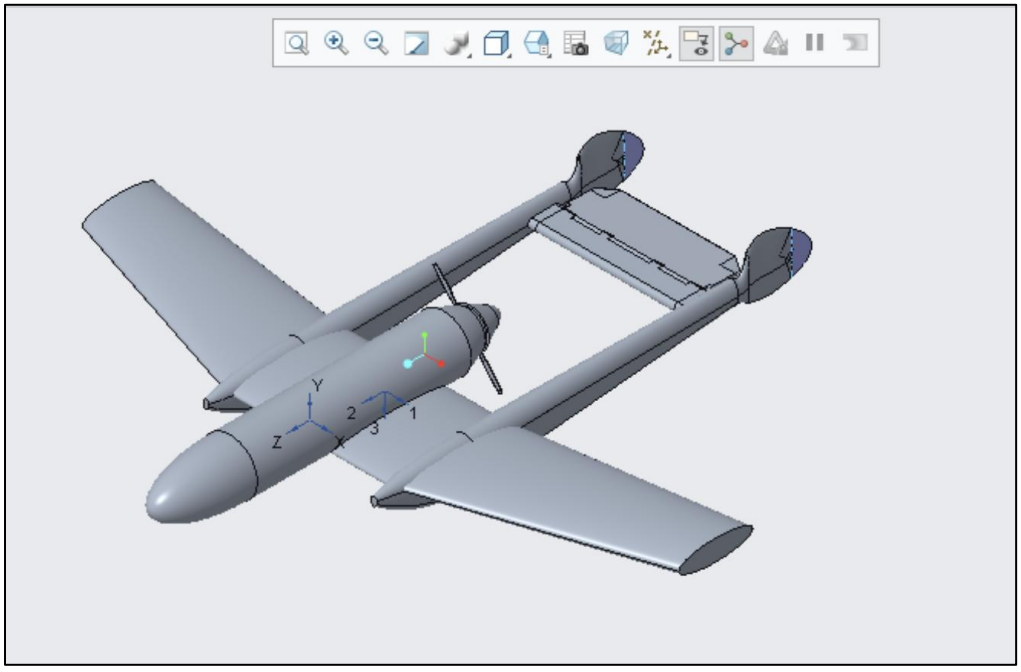

Figure 2: First iteration CAD model of proposed aircraft

Weight Calculations:

- **$W_{payload}$ = 0.27**
  Weight of the Coke can (kg)
- **W_{motor} = 0.119**
  Weight of propeller, motor, and ESC (kg)
- **W_{servo} = 0.009 * 5**
  Weight of control surface motors (kg)
- **$W_{Battery}$ = 0.125**
  Weight of the battery (kg)
- **$W_{Control\ Horns}$ = 0.009 * 6**
  Weight of control horns (kg)
- **W_{foam} = 0.32527**
  Weight of foam utilized in the first CAD model (kg)

Total Weight:

$$w = \left(W_{payload} + W_{motor} + W_{servo} + W_{Control\ Horns} + W_{Battery} + W_{foam}\right) \cdot 9.81 = 9.2044\ N$$

Aerodynamic Parameters and Constants:

- $C_{d0} = 0.03$
  Derived from airfoil tools
- $\rho = 1.225$
  Air density at sea level (kg/m³)
- $\rho_0 = 1.225$
  Air density at sea level (kg/m³)
- $\rho_c = 1.215$
  Density of air at 120 meters altitude (kg/m³)
- $v_{max} = 33$
  Maximum speed of the aircraft (m/s)
- $v_{stall} = 3.878$
  Stall speed based on average human throw power (m/s)
- $ROC = 3.5$
  Rate of climb (m/s)
- $\eta_p = 0.75$
  Propeller efficiency
- $\mu = 1.789 * 10^{-5}$
  Dynamic viscosity of air at sea level (kg/m/s)

Aspect Ratio:

$$AR = \frac{1009.186^2}{244771} = 4.1609$$

Lift-to-Drag Ratio and Aircraft Geometry:

- $C_{L_{max}} = 1$
  Maximum coefficient of lift
- $\left(\frac{L}{D}\right)_{max} = 10$
  Maximum lift-to-drag ratio (L/D max), SAE Aero design states L/D max for RC Aircraft is typically between 8-12
- $e = 0.75$
  Average Oswald efficiency factor for RC aircraft

Induced Drag Factor:

$$k = \frac{1}{\pi \cdot e \cdot AR} = 0.102$$

Wing Loading for Stall:

$$\frac{W}{S} = 0.5 \cdot \rho \cdot v_{stall}^2 \cdot C_{L_{max}} = 9.2113 \ \frac{N}{m^2}$$

Propeller Thrust required to achieve maximum speed (based on propeller efficiency and aerodynamic drag):

$$\left(\frac{W}{P_{SL}}\right) = \left(\frac{W}{S}\right) \frac{\eta_p}{0.5 \cdot \rho \cdot v_{max}^3} \cdot \frac{1}{C_D + k\left(\frac{2}{\rho \cdot v_{max}^2}\right)\left(\frac{W}{S}\right)^2} = 0.0102 \ \frac{N}{W}$$

Power required for Climb Rate (Rate of Climb):

$$\left(\frac{W}{P_{ROC}}\right) = \frac{1}{\frac{ROC}{\eta_p} + \sqrt{\frac{2}{\rho\sqrt{3 \cdot \frac{C_{D_0}}{k}}} \cdot \left(\frac{W}{S}\right)} \left(\frac{1.155}{\left(\frac{L}{D}\right)_{max} \eta_p}\right)} = 0.1895 \ \frac{N}{W}$$

Adjusted Propeller Thrust considering altitude effects:

$$\left(\frac{W}{P_{ROC}}\right) = \frac{\rho_c}{\rho_0} \cdot \frac{1}{\sqrt{\frac{2}{\rho\sqrt{3 \cdot \frac{C_{D_0}}{k}}} \cdot \left(\frac{W}{S}\right)\left(\frac{1.155}{\left(\frac{L}{D}\right)_{max} \eta_p}\right)}} = 1.6217 \ \frac{N}{W}$$

Wing Sizing:

$$S = \frac{W}{\left(\frac{W}{S}\right)} = \frac{9.2044 \ N}{9.2113 \ \frac{N}{m^2}} = 0.99925 \ m^2$$

Power Required:

$$P = \frac{W}{\left(\frac{W}{P_{SL}}\right)} = \frac{9.2044 \ N}{0.0102 \ \frac{N}{W}} = 901.012 \ Watts$$

Fuselage and Tail Sizing:

$$D_{inner \ fuselage} = 0.36 \ m$$

$$D_{outer \ fuselage} = 0.64 \ m$$

$$A_{inner} = 0.1018 \ m^2$$

$$A_{outer} = 0.3217 \ m^2$$

The length of fuselage is generally 75% of wingspan for RC aircraft:

$$h_{fuselage} = 0.75 \cdot \left(\frac{1009.186}{1000}\right) = 0.7569 \ m$$

Volume of interior fuselage:

$$V_{inner} = A_{inner} \cdot h_{fuselage} = 0.0770 \ m^3$$

Volume of exterior fuselage:

$$V_{outer} = A_{outer} \cdot h_{fuselage} = 0.2435 \ m^3$$

Horizontal tail sizing is usually ¼ of the surface area of the wing:

$$S_{t_{horz.}} = 0.25 \cdot S = 0.2498 \ m^2$$

Vertical tail sizing is usually 1/10 of the surface area of the wing:

$$S_{t_{vert.}} = 0.1 \cdot S = 0.0999 \ m^2$$

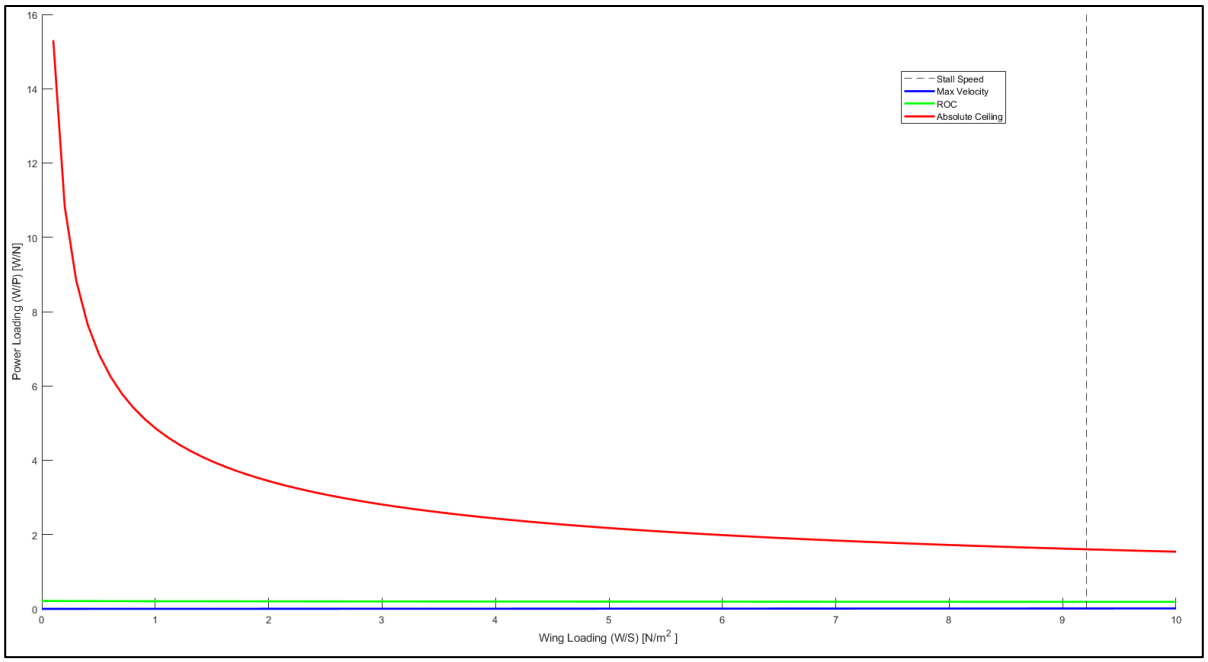

Figure 3: Power Loading vs. Wing Loading

Detailed Design

To build upon the initial design, numerous aspects of the first iteration needed to be revised and redone. The primary reason was due to a better understanding of the scope and direction of the design; namely, with the intent of refining the stability of the initial mockup. Among the first items that were redesigned included the wings and control surfaces, as the first iteration did not feature very complex geometry or properly modeled airfoils. Additionally, to aid in improving the stability of the aircraft, other more minor aspects of the first iteration had to be revised as well, such as adding a greater dihedral angle on the wings and incorporating larger control surfaces to improve flap effectiveness during flight, particularly with the ailerons and rudders. The second design iteration incorporated the information learned from each in-class lecture, as well as feedback from the professor.

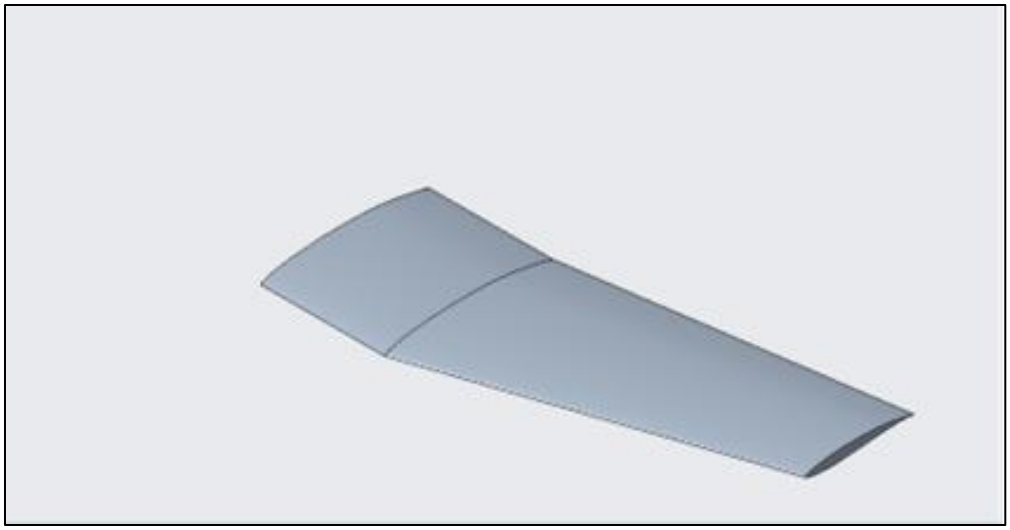

Figure 4: Second Design Iteration of Wing

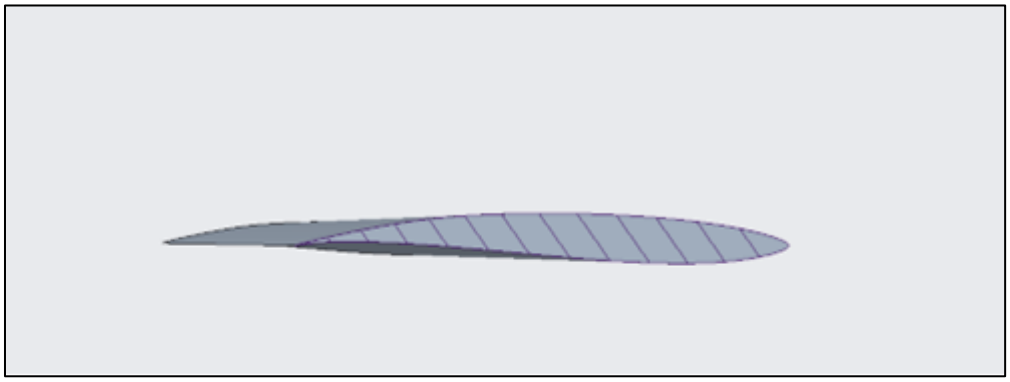

Figure 5: Airfoil Cross-Section of Wing

For the second iteration of the wing design, the Eppler E818 airfoil has been chosen for its strong lift-to-drag ratio, which is essential for improving the airfoil's overall aerodynamic performance. The data values that were used for the calculations have been based on the information provided by Airfoiltools.com. The surface area is calculated to be 350,437 mm^2, accounting for both wings to ensure equal lift distribution across the foil. The decision to go without dihedral further simplifies the design without needing to rely on wing tilt for roll stabilization. Styrofoam remains the material of choice and will be supplied by the HSDC.

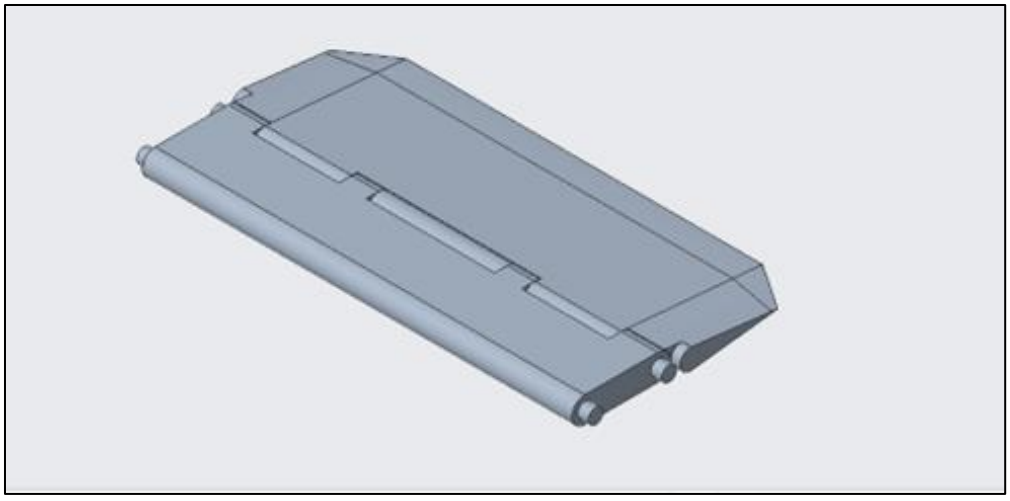

Figure 6: Second Design Iteration of Horizontal Tail

Figure 6 displays the second iteration of the horizontal tail design, which has been modeled with a surface area of 72,942.4 mm². The horizontal tail is located 470.101 mm from the aircraft's Center of Gravity (CG) to help balance the pitching moment and enhance the aircraft's stability. The calculated aspect ratio is 0.82 to minimize drag and improve lift distribution. Styrofoam continues to be the material of choice, and this configuration ensures improved control with pitching motion to maintain attitude during flight.

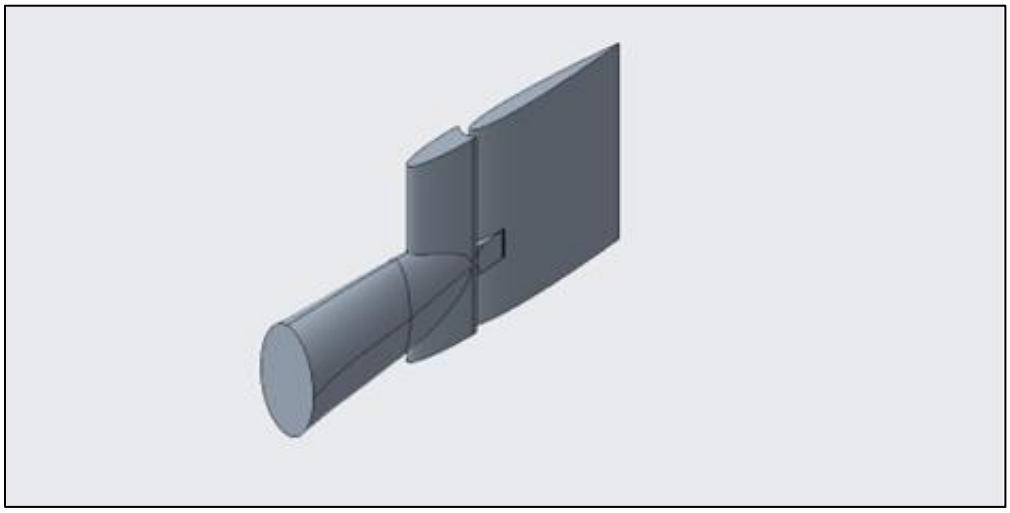

Figure 7: Second Design Iteration of Vertical Tail

Figure 7 displays the second iteration of the vertical tail design, which has been modeled with a surface area of 12,837.8 mm² (note that this is for one vertical tail). The vertical tail is located 574.970 mm from the aircraft's CG, contributing to the overall yaw stability and control. The calculated aspect ratio is 0.38, which helps minimize drag while maintaining sufficient stability for the aircraft's directional control. Styrofoam remains the material of choice, and this

configuration provides enhanced yaw control, improving the aircraft's responsiveness to directional inputs and ensuring stable flight characteristics.

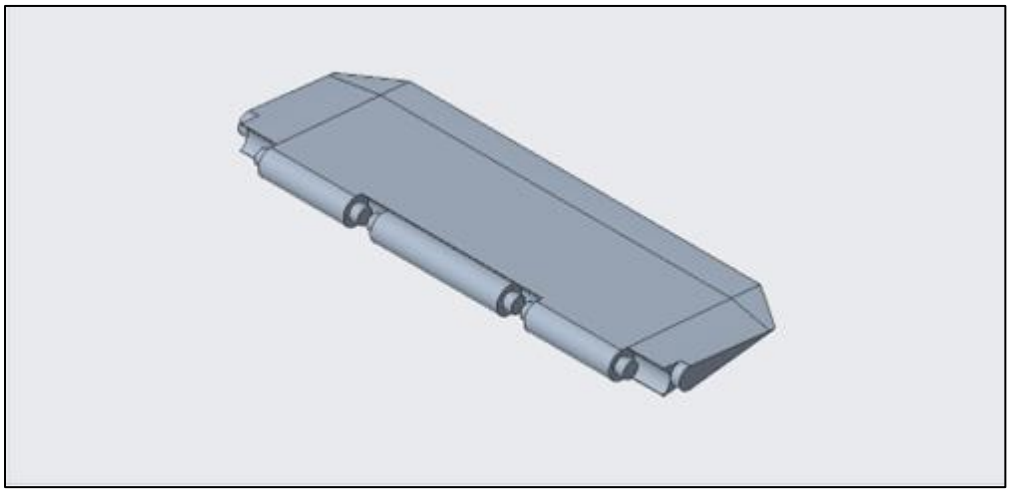

Figure 8: Second Design Iteration of Elevator

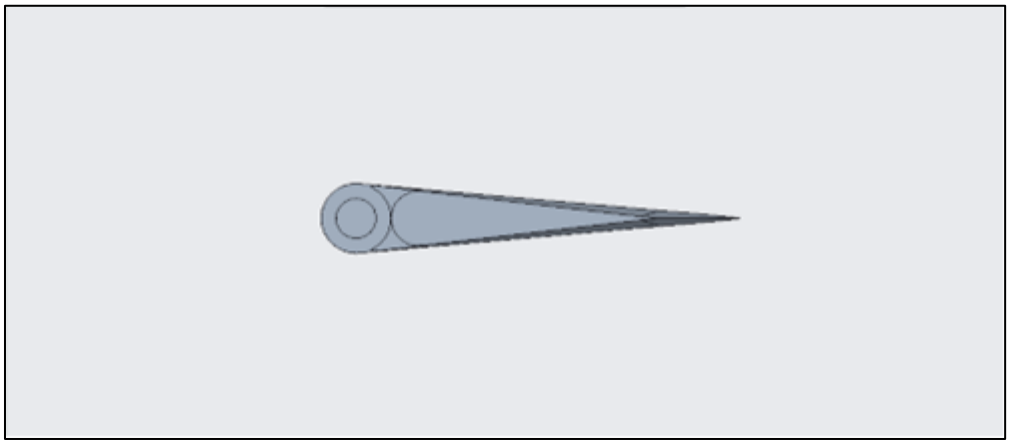

Figure 9: Side-Profile View of Elevator

Figures 8 and 9 display the second iteration of the elevator design, which has been modeled with a surface area of 43,664.9 mm². Styrofoam continues to be the material of choice, and this configuration allows for efficient pitch control, providing effective response to pilot inputs while maintaining the desired attitude during flight.

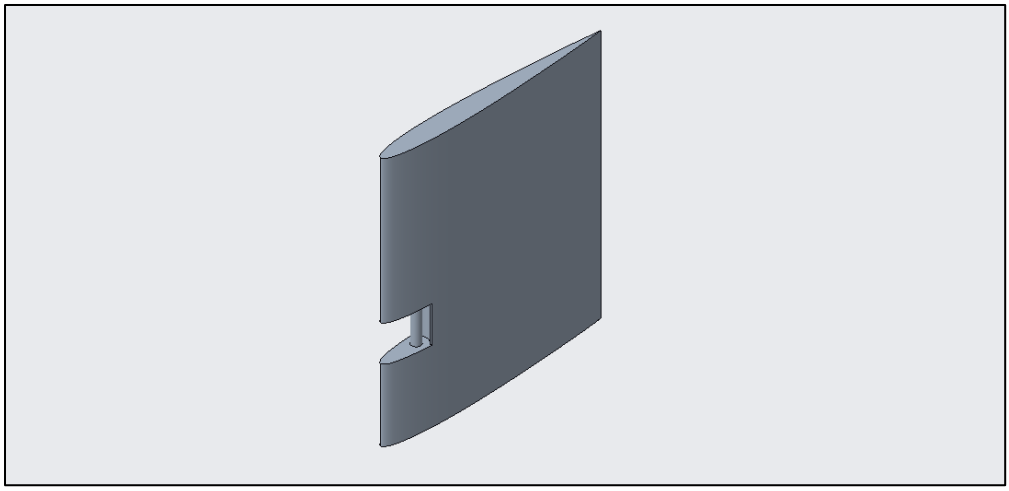

Figure 10: Second Design Iteration of Rudder

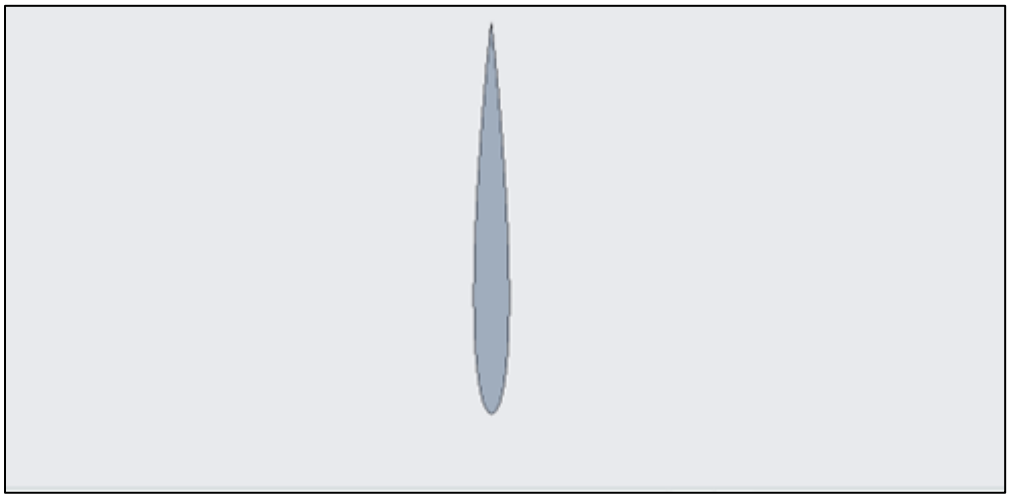

Figure 11: Top-Profile view of Elevator

Figure and Figure 11 display the second iteration of the rudder design, which has been modeled with a surface area of 9,239.26 mm². Styrofoam continues to be the material of choice, and this configuration allows for precise directional control as well as stable yaw characteristics during flight.

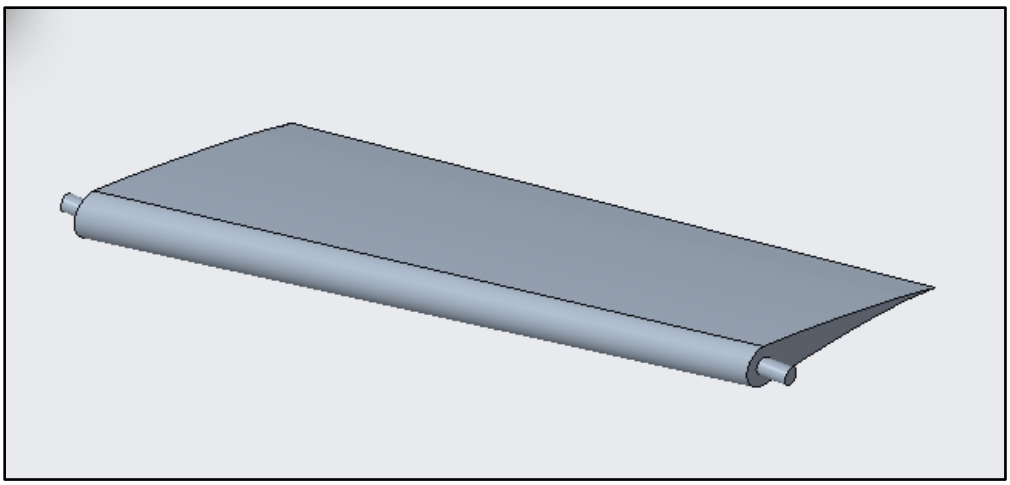

Figure 12: Isometric View of Aileron

Figure 12 shows the current iteration design for the aileron. The current iteration for the aileron design specifies a surface area of roughly 11,377.7 mm² per aileron, accounting for both ailerons, the combined effective surface area is doubled to 22,755.4 mm^2. Styrofoam continues to be the material of choice, and this configuration would allow for adjusting the rolling motion around the longitudinal axis.

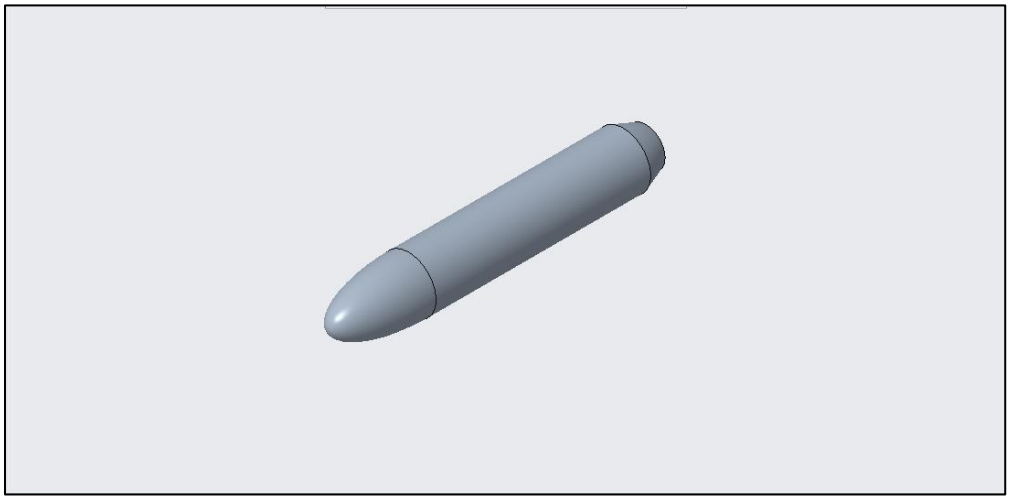

Figure 13: Second Design Iteration of Fuselage

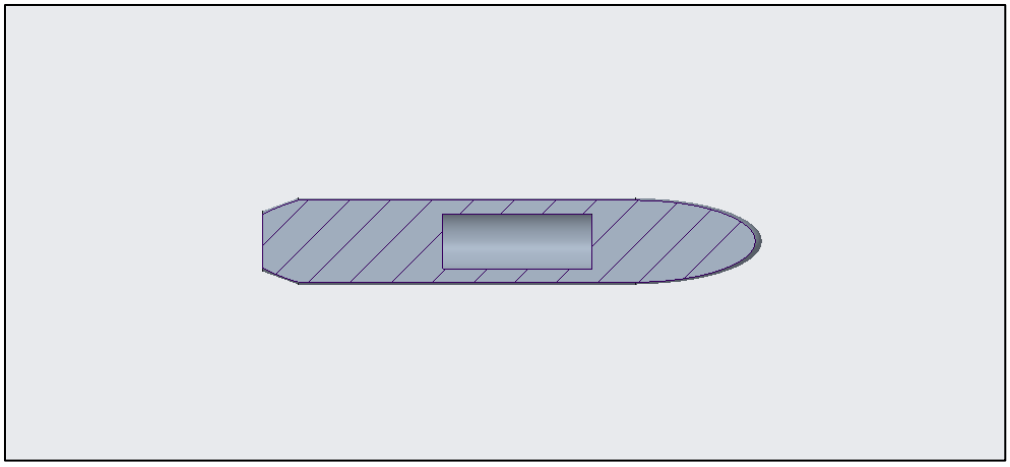

Figure 14: Cutaway View of Fuselage, Displaying Compartment for Payload

Figures 13 and 14 display the second iteration of the fuselage design, including the cutaway for holding the payload. This configuration will allow for utilizing the payload in controlling the flight dynamics, particularly when it comes to stability and maneuverability of the aircraft. Styrofoam continues to be the material of choice, and integrating the payload of the payload in this manner also optimizes weight distribution.

Figure 15: SG90 Mini 9g Micro Servo Motor [3]

A total of 6 SG90 Mini 9g Micro Servo Motors, provided by the professor, will act as the control surface motors. These motors will be evenly distributed by having:

- 2 motors for the rudder to control the yaw, allowing the aircraft to rotate left or right along the vertical axis.
- 2 motors for the elevator to control the pitch, enabling the aircraft to climb or dive along the horizontal axis.
- 2 motors for the ailerons to control the roll, allowing the aircraft to tilt left or right along the longitudinal axis.

The compact size and reliability of the SG90 servos make these motors well-suited for the fuselage, integrating effectively with the payload control systems to achieve precise and responsive flight handling.

Figure 16: 1045 Propeller CW CCW Accessories Kit [1]

For the propeller and motor selection, the professor has provided the abcGoodefg 1000KV RC Brushless Motor A2212 13T with a 30A Brushless ESC and a 1045 Propeller CW CCW Accessories Kit. The 1045 propellers, with a 10-inch diameter and 4.5-inch pitch, generate sufficient thrust for a small RC plane in the weight range of roughly 1.5 to 2.5 kg to maintain stable flight. The 1000KV brushless motor for propulsion allows for balancing between power and efficiency, while the 30A ESC allows for smooth and reliable power delivery.

Figure 17: Blomiky 2 Pack 11.1V 1500mAh 35C Lipo Battery with Deans T Plug for RCAirplane, RC Helicopter, RC Car Truck, RC Boat and Quadcopter Drone 11.1V 1500mAh T 2 [2]

For the battery selection, the professor has provided a Blomiky 2 Pack 11.1V 1500mAh 35C LiPo Battery with Deans T Plug. This battery will provide the necessary amps for the abcGoodefg 1000KV motor. The 35C rating means that the battery can deliver up to 52.5 amps of continuous current, which is more than enough to support the current requirements of the motor and ESC. The 11.1 volts for the voltage rating matches the requirements of the motor, while the 1500 mAh capacity offers a reasonable flight time.

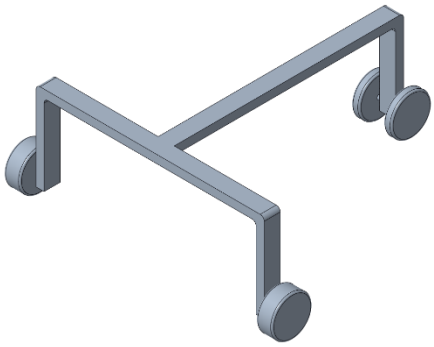

Figure 18: Landing Gear

Figure 18 displays a model of the design of the landing gear. It has two front wheels that serve as the main landing gear to ensure primary support and load-bearing capacity of the aircraft during landing. The rear wheel is positioned closer to the aircraft's CG for stability, as it is perpendicular to the main gear.

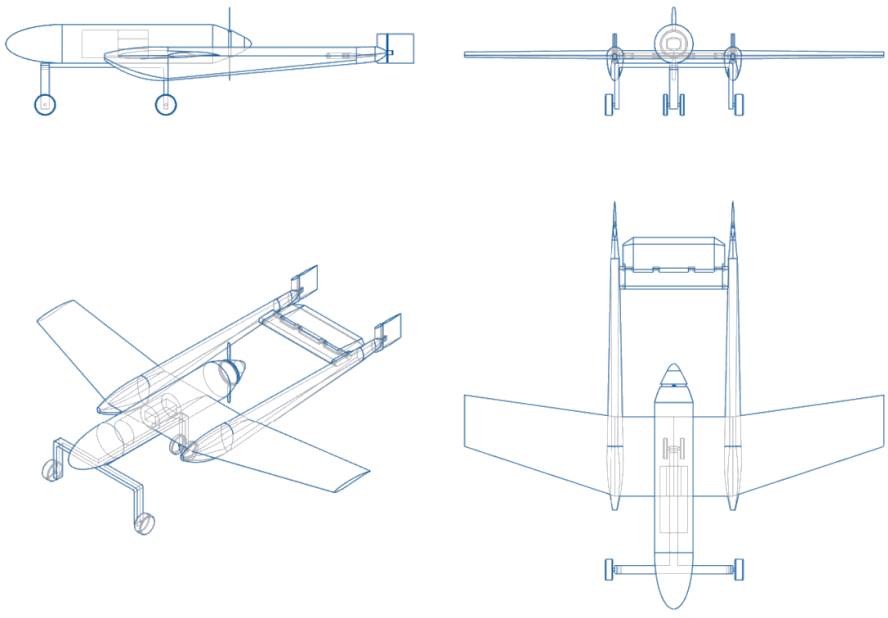

Figure 19: Hidden Line Sketch of Full Assembly

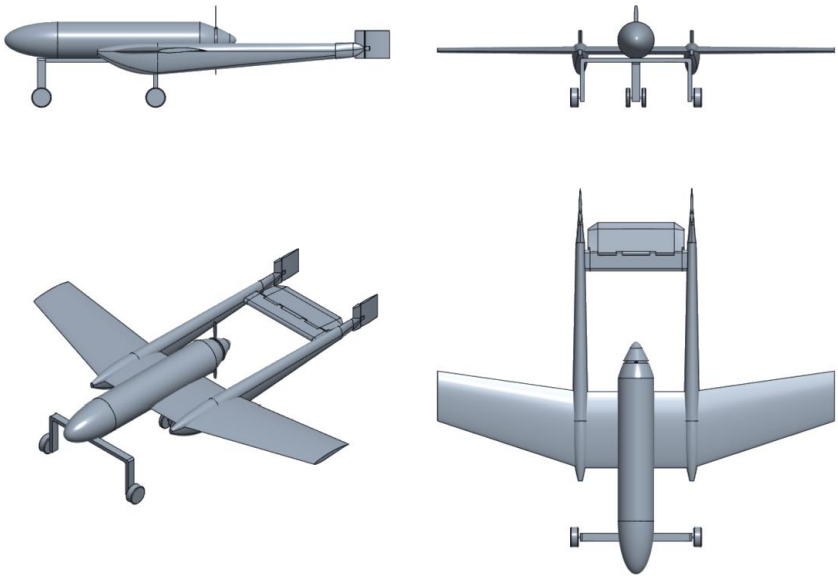

Figure 20: Shaded-Edge Drawing of Full Assembly

Figures 19 and 20 display both the second iteration of the preliminary sketch and CAD model. The hidden line representation shows the internal features and structure not visible in the shaded view, while the shaded version highlights the external geometry and surface details of the full assembly.

Longitudinal Static Stability

Category	Coefficient	Value
X-Force Derivatives	C_{X_u}	-0.0962
X-Force Derivatives	C_{X_α}	0.0296
X-Force Derivatives	$C_{X_{\dot{\alpha}}}$	0.0000
X-Force Derivatives	C_{X_q}	0.0000
Z-Force Derivatives	C_{Z_u}	-0.4714
Z-Force Derivatives	C_{Z_α}	-3.5778
Z-Force Derivatives	$C_{Z_{\dot{\alpha}}}$	-0.6934
Z-Force Derivatives	C_{Z_q}	-2.3115
Pitching Moment Derivatives	C_{m_u}	-0.0168
Pitching Moment Derivatives	C_{m_α}	-0.1469
Pitching Moment Derivatives	$C_{m_{\dot{\alpha}}}$	-2.0362
Pitching Moment Derivatives	C_{m_q}	-6.7674
Pitching Moment Derivatives	C_{m_0}	0.0578

Table 4: Longitudinal Stability Coefficients

From Table 4, the results of the longitudinal stability coefficients are shown. To satisfy the longitudinal static stability, the pitching moment with respect to angle of attack needs to have a negative trend $\left(C_{m_\alpha} < 0\right)$. The other condition that needs to be met is that the pitching moment at zero angle of attack needs to be positive to achieve longitudinal static stability $\left(C_{m_0} > 0\right)$. The results show that the pitching moment has a negative trending slope $\left(C_{m_\alpha} = -0.2513\right)$ and the pitching moment at zero angle of attack is greater than zero $\left(C_{m_0} = 0.0423\right)$.

$$\left(C_{m_0} = 0.0423\right).$$

$$C_{m_\alpha} = C_{L_\alpha}\left(h - h_{n_{wb}}\right) - C_{L_{\alpha_t}}\overline{V_H}\left(1 - \frac{\partial\epsilon}{\partial\alpha}\right) = -0.2513$$

$$C_{m_0} = C_{m_{ac_{wb}}} + C_{m_{0_p}} + C_{L_{\alpha_t}}\overline{V_H}(\epsilon_0 + i_t)\left[1 - \frac{S_t}{S}\frac{C_{L_{\alpha_t}}}{C_{L_{\alpha_w}}}\left(1 - \frac{\partial\epsilon}{\partial\alpha}\right)\right] = 0.0423$$

Other equations were obtained and followed carefully from Dr. Robert C. Nelson *Flight Stability and Automatic Control,* table 3.3 [4].

Lateral Static Stability

$\rho = 1.225$ $(kg/m3)$	$S = 0.335057$ $(Wing\ area\ in\ m^2)$
$V = 33$ $(maximum\ velocity\ in\ m/s)$	$l_t = 0.44$ $(Tail\ moment\ arm\ in\ meters)$
$S_t = 0.0687$ $(Vertical\ tail\ area\ in\ m^2)$	$\bar{c} = 0.192$ $(Mean\ aerodynamic\ chord\ in\ meters)$
$V_v = \frac{S_t l_t}{S\bar{c}} = 0.4699$ $(Vertical\ fin\ volume\ ratio)$	$\frac{d\sigma}{d\beta} = 0.5$ $(Sidewash\ Gradient)$
$\eta_t = 0.8$ $(Tail\ efficiency\ factor)$	$V_{stall} = 3.878$ (m/s)
$V_{max} = 33$ (m/s)	$a_{SL} = 340$ $(Speed\ of\ sound\ at\ sea\ level\ in\ m/s)$
$Maximum\ Mach\ Number = \frac{V_{max}}{a_{SL}} = 0.097$	$Minimum\ Mach\ Number = \frac{V_{stall}}{a_{SL}} = 0.011$
$C_{n\beta} > 0\ for\ lateral\ stability$[6]	$\alpha_f = -5°\ to\ 5°$ $(range\ of\ angle\ of\ attack\ values)$
$\beta = 0°\ to\ 3°$ $(range\ of\ sidewash\ angle\ values)$	$a_f = 0.02°$ $(Lift\ slope\ of\ vertical\ fin)$
$a_r = 2\pi\ (Lift\ slpe\ of\ rudder)$	$\delta_r = -24°to\ 24°$ $(range\ of\ rudder\ deflection\ angles)$

Table 5: List of parameters for proposed aircraft design

The lift slope for the vertical tail surface is:

$$C_{L_F} = a_F(-\beta + \sigma) + a_r\delta_r$$

The maximum C_{L_F} was determined to be = 0.046

Lift for the vertical tail surface is:

$$L_F = C_{L_F}\frac{\rho}{2}V_F^2 S_F$$

Assuming $\alpha_f = 5°$ and $\delta_r = 24°$,

$$L_F = 2.1603\ N$$

[6] For commercial aircraft, C_{n_β} is typically between 0.05 and 0.4 according to the University of Sevilla [5].

The yawing moment for the vertical tail surface is:

$$N_F = -C_{L_F} \frac{\rho}{2} V_F^2 S_F l_F$$

Assuming $\alpha_f = 5°$ and $\delta_r = 24°$,

$$N_F = -0.926\ Nm$$

The yawing moment coefficient is:

$$C_{n_F} = -V_V C_{L_F} \left(\frac{V_F}{V}\right)^2$$

Assuming difference in relative air speed for fuselage and vertical tail's is negligible:

$C_{n_F} = -0.0216$

Contribution to weathercock stability:

$$\frac{\partial C_{n_F}}{\partial \beta} = V_V \frac{\partial C_{L_F}}{\partial \beta} \eta_F \left(1 + \frac{\partial \sigma}{\partial \beta}\right) = V_V a_F \eta_F \left(1 + \frac{\partial \sigma}{\partial \beta}\right)$$

$\frac{\partial C_{n_F}}{\partial \beta} = 6.5608 * 10^{-5}$

Range of values for roll angle about axis:

$$\phi = 0° \ to\ 25°$$

Assuming $\alpha_x = 5°$, sideslip velocity is (condition set $\phi = 12.5^{\circ}$):

$v = V_{max} \sin \alpha_x \sin \phi$

$$v = (33) \sin\left(5 \cdot \frac{\pi}{180}\right) \sin\left(12.5 \cdot \frac{\pi}{180}\right)$$

$$v = 0.6225$$

The sideslip angle can be calculated via:

$$\beta = \sin^{-1}\left(\frac{v}{V}\right) \rightarrow \beta_{max} = 2.1109°$$

Taking a typical value for dihedral angle of 4 degrees, the restoring moment roll coefficient is:

$$\Delta C_l = C_{l_\beta}\ \alpha_x\ \phi_{max} \rightarrow \Delta C_l = 0.0027$$

And the Roll stiffness C_{l_ϕ} thus is:

$$C_{l_\phi} = C_{l_\beta}\ \alpha_x \rightarrow C_{l_\phi} = 0.0061$$

The change in coefficient of lift with respect to rudder deflection angle is given as:

$$\Delta C_{l_\beta} = -a_F \left(1 + \frac{\partial \sigma}{\partial \beta}\right) \frac{S_F z_F}{Sb} \left(\frac{V_F}{V}\right)^2$$

However, $\Delta C_{l_\beta} = 0$ as the m.a.c of the vertical tail is in line with the CG of the plane. The calculations performed have implemented core aerodynamic relationships (i.e. lift slope of the vertical tail, tail volume ratio, sidewash gradient, and tail efficiency) to compute both the yawing-moment coefficient produced by sideslip and its corresponding slope with respect to sideslip. The positive contribution to weathercock stability confirms a restoring yawing moment, and when nondimensionalized by dynamic pressure, wing area, and mean chord it falls within the 0.05-0.4 range typical in commercial aircraft design [5]. Quantifying the roll stability through the dihedral effect shows that the sideslip combined with the 5° dihedral creates a positive roll-restoring moment. By verifying the aircraft's geometry, the team has been able to calculate the stability derivatives to represent an accurate approach in analyzing the aircraft's lateral stability.

Manufacturing Plan

- 3D-Printed booms with wooden internal supports (internal wooden beams with a 3D-printed shell).
- Foam fuselage with Monokote wrapping.
- Foam wings to be made using the foam cutter at the HSDC.
- 3D-printed rudder and elevator tail with wooden rods and hinges for support.
- 3D-printed attachment for motor and propeller to fuselage.
- Carbon fiber rods for the wings.
- Carbon fiber hinges for ailerons and simple wooden ribs for connectors to the main rods.
- Gorilla wood glue for wood-to-foam attachments.
- Epoxy used for 3D-to-3D attachments.
- Superglue for 3D-to-carbon fiber attachments.
- Threaded screws and inserts for wood-to-3D attachments.
- If needed, slight adjustments to the frame to allow for slotted fits, i.e., wood-to-3D or wood-to-wood.

Rationale:

- The 3D printing is for design elements of the aircraft that would be either complex or tedious to machine/fabricate by hand, such as the shape of the booms. And 3D printing the control surfaces would make them sturdier than foam during flight and operation. Additionally, using a filament with a high heat resistance for the motor attachment would be ideal for any excessive heat generated by the motor and propeller during operation.
- Foam and wooden design elements were chosen for the purposes of convenience, ease of use/application, and cost for the overall design.
- Carbon fiber was selected as a material of choice for the wing and aileron support due to it being a more durable material than wood; while it is more expensive, for the purposes of reinforcing the wings and ensuring that they will be able to withstand the anticipated forces and loads during flight, it was determined that carbon fiber supports would be better suited for the manufacturing plan.

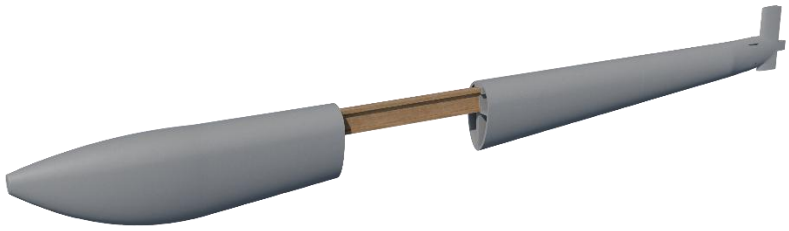

Figure 21: Wing boom modeled with wooden I-beam support

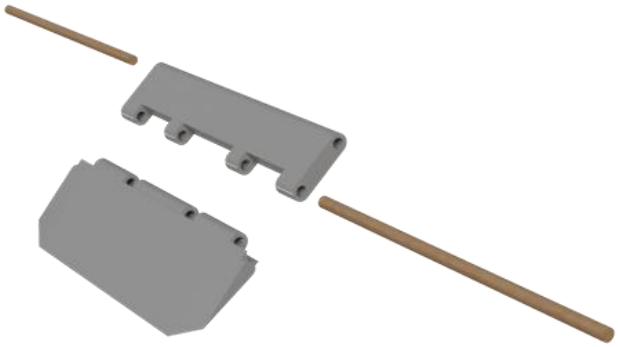

Figure 22: Elevator modeled with wooden rod supports

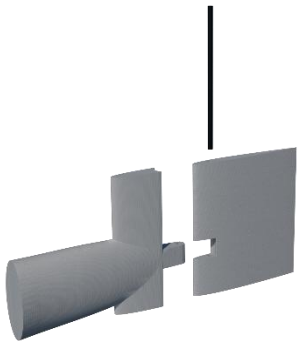

Figure 23: Elevator modeled with wooden rod supports

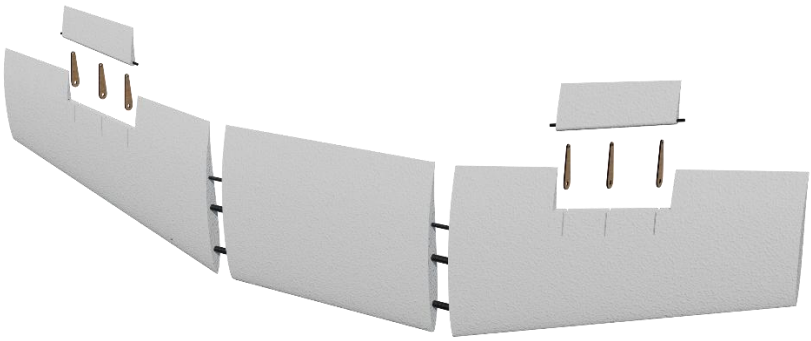

Figure 24: Exploded view of wings, ailerons and wooden attachments for manufacturing

Figure 25: Exploded view of fuselage, 3D printed motor mount and motor

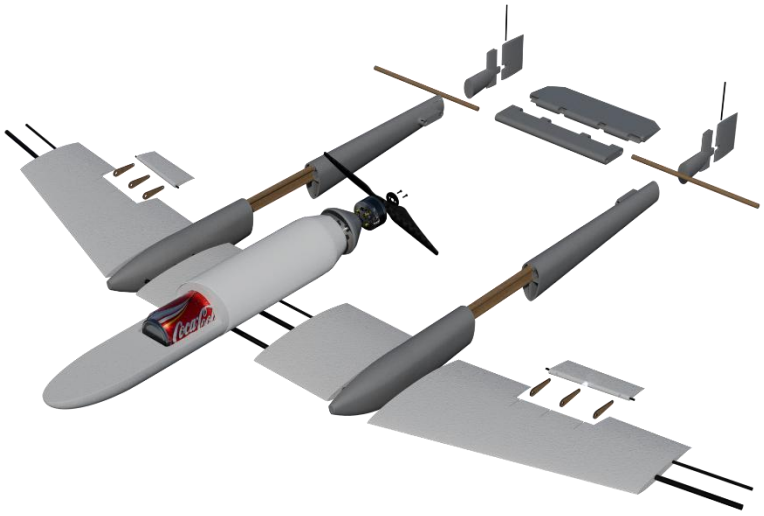

Figure 26: Exploded view of entire assembly

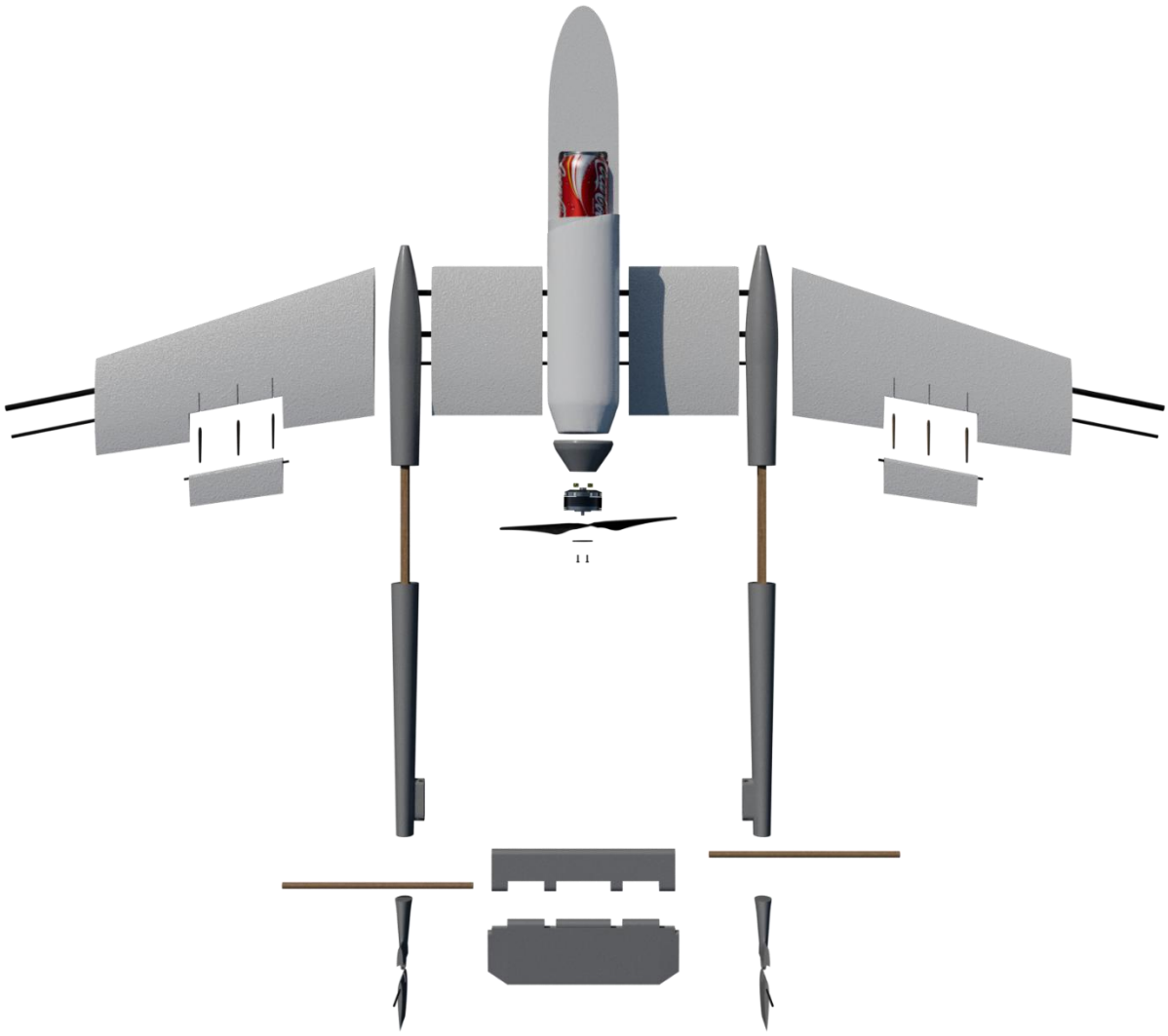

Figure 27: Exploded top view of entire assembly

Longitudinal Dynamic Stability

Longitudinal Derivatives

Longitudinal force derivative with respect to velocity:

$$C_{X_u} = -\left(C_{D_u} + 2C_{D_0}\right) + C_{T_u}$$

Lift coefficient derivative with respect to velocity (Mach-dependent):

$$C_{L_u} = \left(\frac{M^2}{1 - M^2}\right) C_L$$

Pitching moment derivative with respect to velocity (Mach-dependent):

$$C_{m_u} = M \cdot \frac{dC_m}{dM}$$

Pitch Rate Derivatives

Vertical force derivative with respect to pitch rate:

$$C_{Z_q} = -2C_{L_{\alpha_t}} \eta \overline{V}_H$$

Pitching moment derivative with respect to pitch rate:

$$C_{m_q} = -2C_{L_{\alpha_t}} \eta \overline{V}_H \left(\frac{l_t}{\overline{c}}\right) \cdot 1.1$$

Angle of Attack Derivatives

Vertical force derivative with respect to angle of attack:

$$C_{Z_\alpha} = -2\overline{V}_H C_{L_{\alpha_t}} \eta_h \left(\frac{\partial \varepsilon}{\partial \alpha}\right)$$

Pitching moment derivative with respect to angle of attack:

$$C_{m_\alpha} = -2\overline{V}_H \eta_h C_{L_{\alpha_t}} \left(\frac{l_t}{\overline{c}}\right) \left(\frac{\partial \varepsilon}{\partial \alpha}\right)$$

Vertical force derivative with respect to elevator deflection:

$$C_{Z_{\delta_e}} = -\left(\frac{S_t}{S}\right) \eta_h \frac{\partial C_{L_t}}{\partial \delta_e}$$

Pitching moment derivative with respect to elevator deflection:

$$C_{m_{\delta_e}} = -\eta_{h\overline{V}_H} \frac{\partial C_{L_t}}{\partial \delta_e}$$

Phugoid Mode

Eigen Vales: -0.15 ± 0.491

Natural Frequency: $\omega_n = 0.5134$ rad/s

Damping Ratio: $\zeta = 0.29$

Period: T = 12.8 s

Damped Natural Frequency: $\omega_d = \pm 0.49$

-0.9934 + 0.0000i	-0.9934 - 0.0000i
0.0982 - 0.0024i	0.0982 + 0.0024i
-0.0268 + 0.0005i	-0.0268 - 0.0005i
0.0162 + 0.0496i	0.0162 - 0.0496i

Table 6: Phugoid Mode Eigenvalues

The top row corresponds to the changes in forward velocity (u) and vertical velocity (w). The middle rows show the pitch rate (q) and the bottom row shows the pitch angle (θ). This shows that there are slow, oscillating exchanges in speed and altitude with large changes in forward and vertical velocity and pitch rate and angle having little effect.

Short Mode

Eigen Vales: -17.3417 ± 0.0000i

Natural Frequency: ω_n = 17.34 rad/s

Damping Ratio: ζ = 1

Period: T = Indefinite

Damped Natural Frequency: ω_d = ± 0.00

0.0219 + 0.0000i	0.0219 - 0.0000i
-0.9976 + 0.0000i	-0.9976 - 0.0000i
0.0657 + 0.0000i	0.0657 - 0.0000i
-0.0038 + 0.0000i	-0.0038 - 0.0000i

Table 7: Short Mode Eigenvalues

With reference to Table 7, the top row of indicates the forward velocity and shows little change. The second row shows that there is strong pitching motion due to large changes in vertical velocity, The third row indicates that the pitch rate is low with quick damping and the last row shows fast pitch up and pitch down oscillations with low changes in speed.

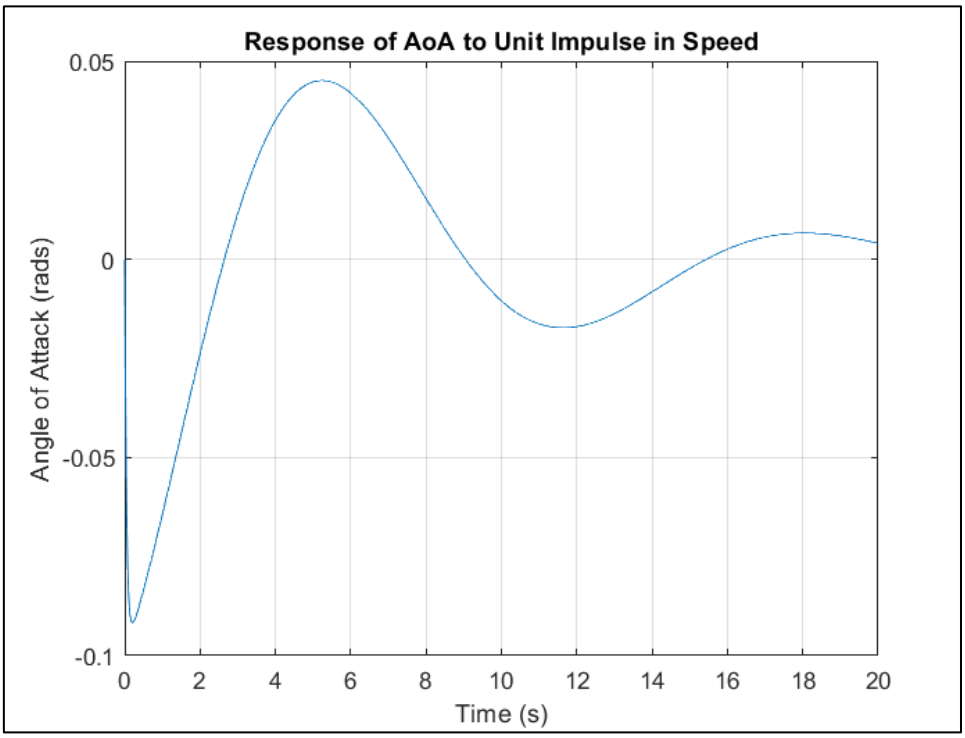

Figure 28: Response of Angle of Attack to Unit Impulse

Figure 28 shows that a unit impulse (i.e. a sudden elevator deflection) produces an almost instantaneous, sharp jump in angle of attack due to the heavily damped short-period mode ($\omega_n \approx 17$ rad/s, $\zeta \approx 1$), which then undergoes one or two rapid oscillations of roughly 0.36 seconds period before dying out. As the fast swings fade, the much slower phugoid mode ($\omega_n \approx 0.51$ rad/s, $\zeta \approx 0.29$, $T \approx 12.8$ s) emerges. This causes broad, lightly damped oscillations as the aircraft trades forward speed for altitude and back. The resulting $\alpha(t)$ curve is the sum of a quick, small-amplitude short-period response superimposed on a long-period, slowly decaying phugoid waveform.

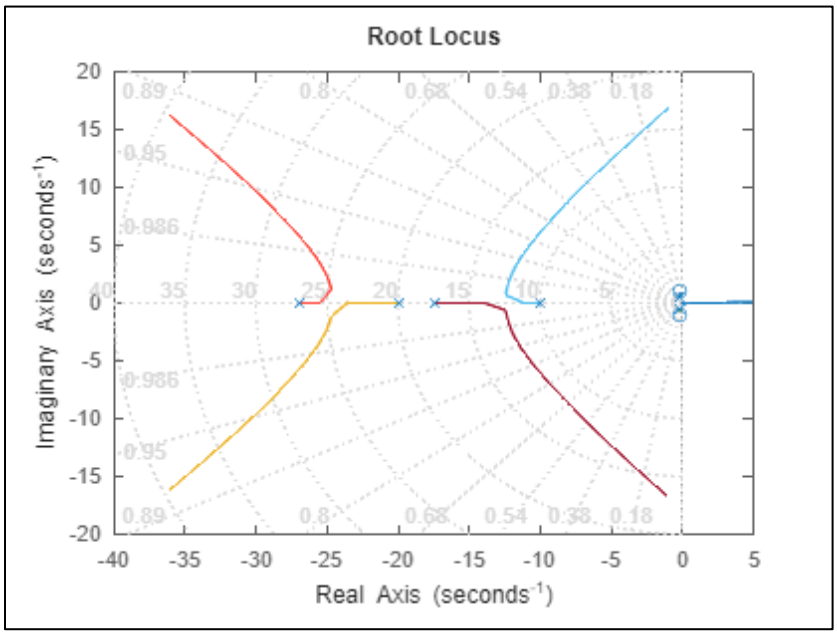

Figure 29: Root Locus with filtered out Angle of Attack

The root locus plot in Figure 29 shows how the two longitudinal modes (i.e. the fast short-period pair and the slow phugoid pair) shift as the closed-loop elevator gain is increased. At zero gain, designated as the "x" marks, the short-period poles lie well left on the real axis with a small imaginary part (this produces high natural frequency, heavy damping) and the phugoid poles lie near the origin with low damping.

As the gain climbs, the short-period branch (the colored curve that sweeps into the upper and lower quadrants) moves outward along the constant-damping contours. This produces more oscillatory behavior before eventually returning toward the real axis along the asymptotes. This translates to the gain to land these poles in the $\zeta \geq 0.5$ region for a critically damped pitch response. The phugoid poles (the branch nearer the origin) slides leftward on the real axis, increasing their negative real part.

As the long-period speed/altitude oscillation decays faster without introducing significant new oscillations, there are explicit trade-offs between rapid, well-damped pitch motion (short period), and desirable phugoid damping when tuning the elevator feedback.

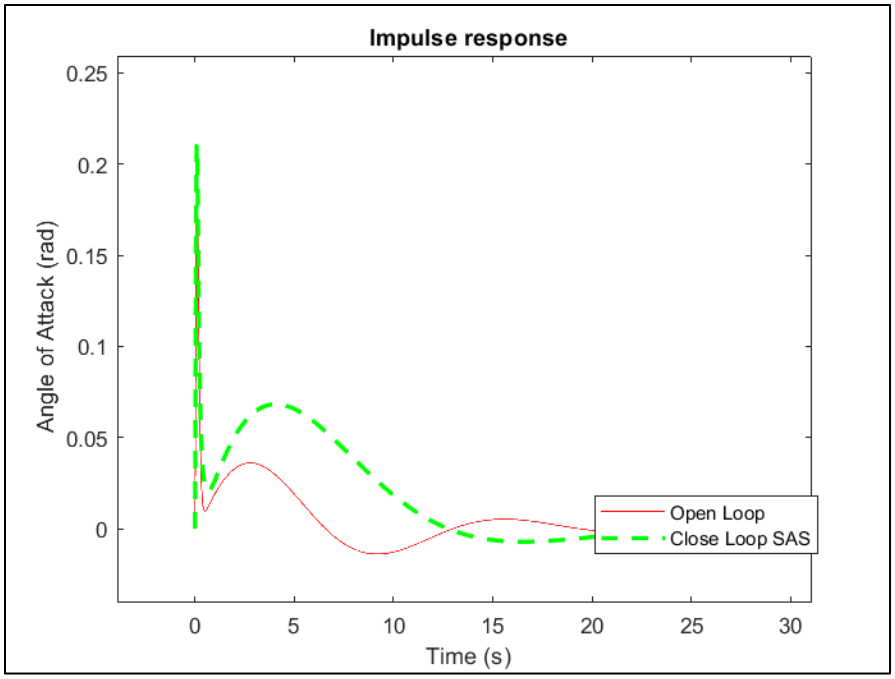

Figure 30: Impulse Response comparison between Open Loop and Closed Loop SAS

In Figure 30, when looking at the open-loop case, the angle of attack shows only a small initial deflection followed by a 12 to 13 s phugoid that decays slowly. With the SAS closed loop, a more prominent short-period spike (≈ 0.2 rad) occurs within the first second and is rapidly damped out. The subsequent phugoid under SAS peaks higher (≈ 0.07 rad) and decays more quickly, yielding a two-stage fast-then-slow transient.

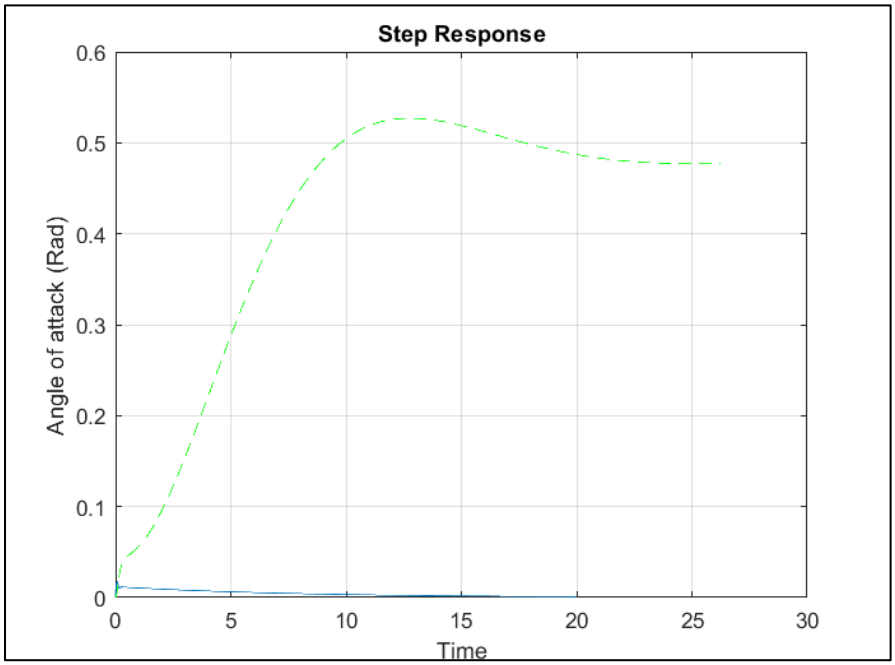

Figure 31: SAS Step Response for Angle of Attack

Figure 31 displays the angle-of-attack step response to a sudden elevator deflection, comparing open-loop (thin blue) and closed-loop SAS (thick green). Under SAS, α ramps up to about 0.52 rad with only a small overshoot and then settles around 0.48 rad, exhibiting almost no oscillation. In the open loop, the angle of attack barely changes, indicating negligible response without the stability augmentation.

Lateral Dynamic Stability

Lateral Derivatives

Lateral force derivative with respect to roll rate:

$$C_{y_p} = C_L \cdot \frac{(AR + \cos(\delta))}{(AR + 4\cos(\delta))} \tan(\delta)$$

Rolling moment derivative with respect to roll rate:

$$C_{l_p} = -\left(\frac{C_{L_\alpha}}{12}\right) \cdot \left(\frac{(1 + 3\lambda)}{(1 + \lambda)}\right)$$

Side force derivative with respect to yaw rate:

$$C_{l_r} = \frac{1}{4} C_{L_0} + 2\left(\frac{l_v}{b}\right)\left(\frac{z_v}{b}\right) C_{L_{\alpha_v}}$$

Yawing moment derivative with respect to yaw rate:

$$C_{N_r} = -2\eta_v \cdot \overline{V}_v \left(\frac{l_t}{b}\right) C_{L_{\alpha_v}}$$

Rolling moment derivative with respect to aileron deflection:

$$C_{l_{\delta_\alpha}} = \frac{2C_{L_{\dot{\alpha}}}\tau}{Sb} c_{root} \cdot \left(\frac{1}{2} dy_\alpha^2 + \frac{2}{3} dy_\alpha \left(\frac{\lambda - 1}{b}\right)\right)$$

Yawing moment derivative with respect to aileron deflection:

$$C_{N_{\delta_\alpha}} = 2K \cdot C_{L_0} \cdot C_{l_{\delta_\alpha}}$$

Rolling moment derivative with respect to rudder deflection:

$$C_{l_{\delta_r}} = \left(\frac{S_v}{S}\right)\left(\frac{z_v}{b}\right)\tau \cdot C_{L_{\alpha_v}}$$

Yawing moment derivative with respect to rudder deflection:

$$C_{N_{\delta_r}} = -V_v \eta_v \tau \cdot C_{L_{\alpha_v}}$$

Rolling moment derivative with respect to sideslip angle:

$$C_{l_\beta} = -V_v \eta_v \tau \cdot C_{L_{\alpha_v}}$$

Dutch-Roll Mode

Eigen Values: -13.977 ± 31.2099

Natural Frequency: ω_n = 34.20 rad/s

Damping Ratio: ζ = 0.41

Period: T = 0.20 s

Damped Natural Frequency: ω_d = ± 31.2099

-0.9934 + 0.0000i	-0.9934 - 0.0000i
0.0982 + 0.0024i	0.0982 - 0.0024i
-0.0268 + 0.0005i	-0.0268 - 0.0005i
0.0162 + 0.0496i	0.0162 - 0.0496i

Table 8: Dutch-Roll Mode Eigenvalues

The top row of the eigen vector contributes primarily to the β values of the lateral dynamic stability which can be interpreted as the "side to side" motion of the aircraft during a Dutch Roll Mode. The middle two rows characterize the yaw and roll motion of the aircraft during a Dutch Roll Mode (r and p). While the bottom row characterizes the banking movements of the aircraft (φ).

Roll Convergence Mode

Eigen Value: -94.57

Time Constant: 0.0106 s

Spiral Mode

Eigen Value: -0.1284

Time Constant: 7.786 s

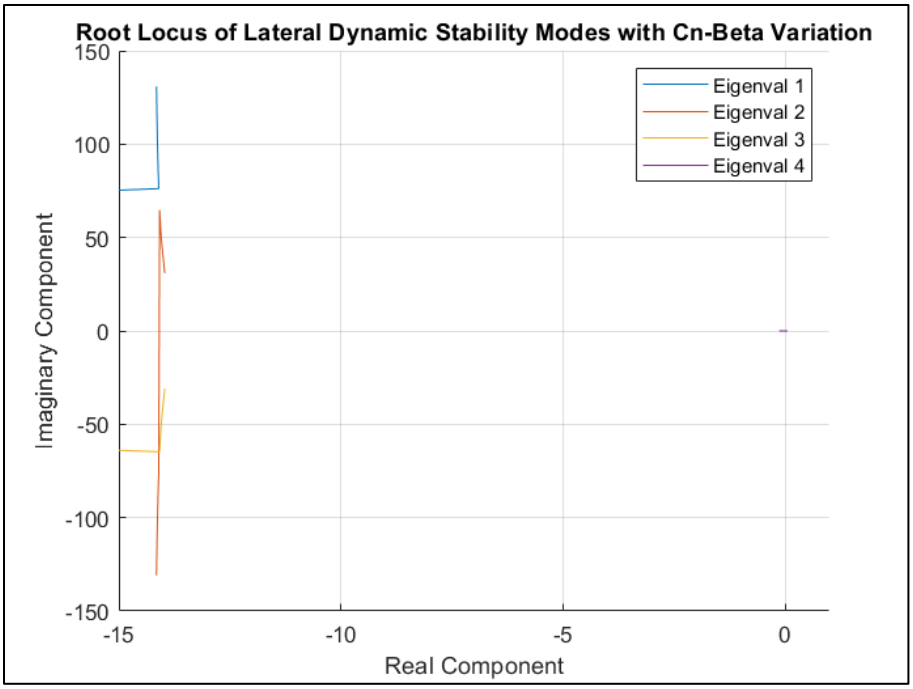

Figure 32: Root Locus of Lateral Dynamic Stability Modes with Cn-Beta Variation

The root-locus plot, seen in Figure 32, shows four lateral-stability poles that increase the directional-stability derivative C_{n_β} (from leftmost crosses toward the colored curves). The blue and orange curves trace the complex-conjugate Dutch-roll pair: starting at high imaginary frequencies (around ± 130 s^{-1} and ± 50 s^{-1}) with modest negative real parts, then swing leftward (more negative real) and inward (lower imaginary) as C_{n_β} grows. This indicates that the oscillation slows slightly, but it also becomes more heavily damped.

The yellow branch is the roll-convergence pole; it remains essentially on the imaginary-zero axis at a large negative real value (≈ –13 s^{-1}) with only a tiny horizontal shift, reflecting that roll-rate damping is unaffected by C_{n_β}. The purple locus curve is the spiral mode: it begins very near the origin due to weak stability and slides left along the real axis, gaining faster, non-oscillatory decay as C_{n_β} increases. Boosting C_{n_β} both damps out the Dutch-roll oscillation and cures spiral slowness, while leaving the roll-convergence pole essentially unchanged.

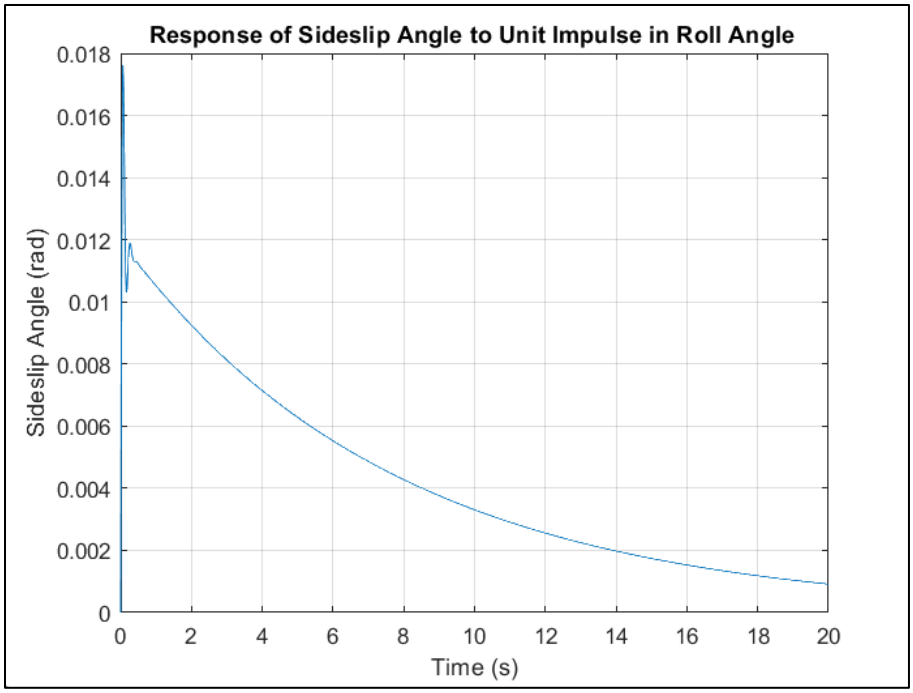

Figure 33: Response of Sideslip Angle to Unit Impulse

Figure 33 shows a unit-impulse disturbance in sideslip produces a rapid, lightly damped oscillation at the Dutch-roll frequency ($\omega_n \approx 34.2$ rad/s, $T \approx 0.20$ s, $\zeta \approx 0.41$). This causes one or two high-frequency swings in β within the first half-second. As the roll-convergence mode has a very short time constant ($\tau \approx 0.0106$ s), its non-oscillatory decay is essentially instantaneous and does not appear as a separate feature. After the Dutch-roll oscillations subside, the much slower spiral mode ($\tau \approx 7.79$ s) governs the remaining drift of β, causing a gentle exponential return toward zero over several seconds. The complete $\beta(t)$ trace is the superposition of a fast, oscillatory Dutch-roll response riding atop a gradual, non-oscillatory spiral decay.

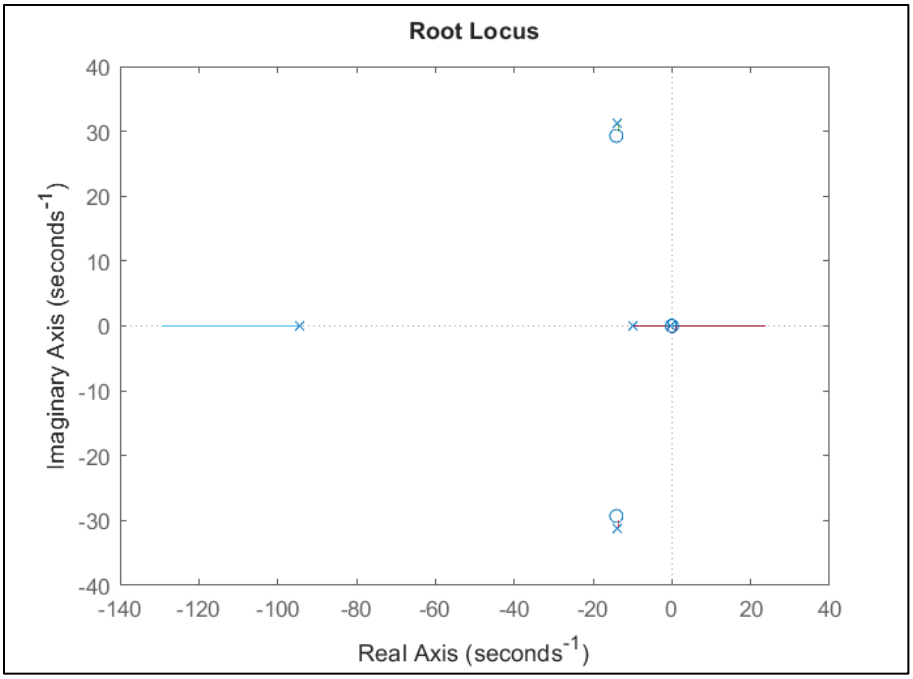

Figure 34: Root Locus on roll rate feedback

Figure 34 displays the root-locus plot on the effect of increasing roll-rate feedback gain on all four lateral-stability poles. At zero gain, the Dutch-roll pair sits at about $-13.98 \pm 31.21\ s^{-1}$, the spiral pole being left of the origin ($-0.13\ s^{-1}$), with the roll-convergence pole left near $-94.6\ s^{-1}$. As the feedback gain increases, the Dutch-roll loci (i.e. the complex-conjugate blue/red curves) sweep further into the left half–plane. The real parts become more negative (a consequence of greater damping) while imaginary parts shrink due to lower oscillation frequency.

The roll-convergence pole (the branch starting at $-95\ s^{-1}$) also moves left, indicating much faster non-oscillatory roll damping. The spiral pole (the near-zero real branch) barely shifts, showing that pure roll-rate feedback has minimal impact on the slow, non-oscillatory spiral mode.

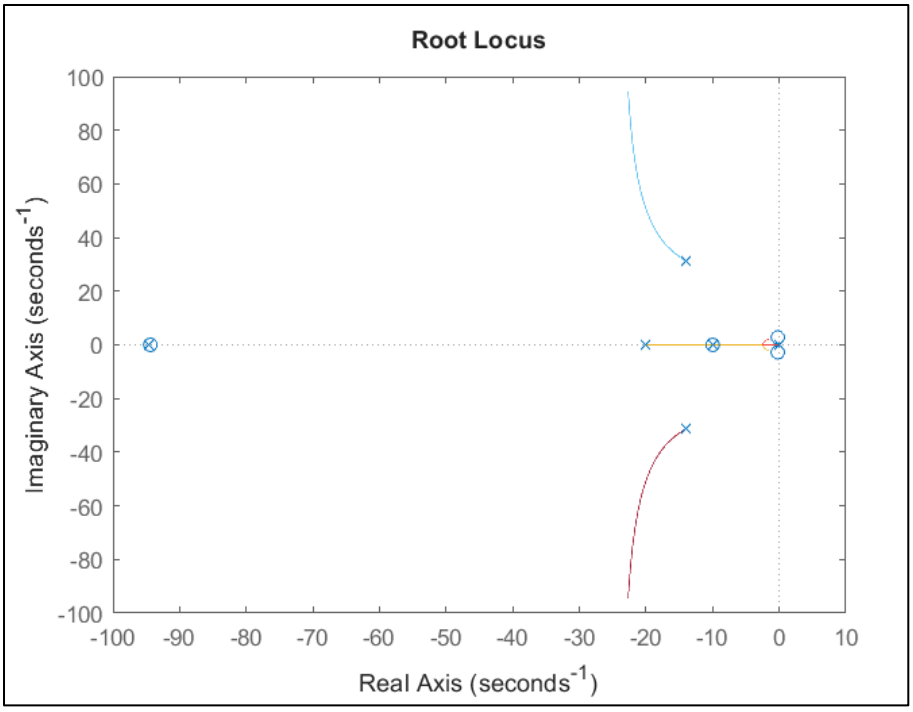

Figure 35: Root Locus on yaw rate feedback

Figure 35 displays the root locus plot of the yaw rate feedback and how moving the gain influences the four lateral poles on the s-plane. The Dutch-roll pair (blue/red loci) sweeps further into the left half-plane, while the roll-convergence pole remains essentially fixed near –95 s^{-1} and the spiral pole stays close to the origin. The yaw-rate feedback chiefly damps Dutch roll with little impact on the other modes.

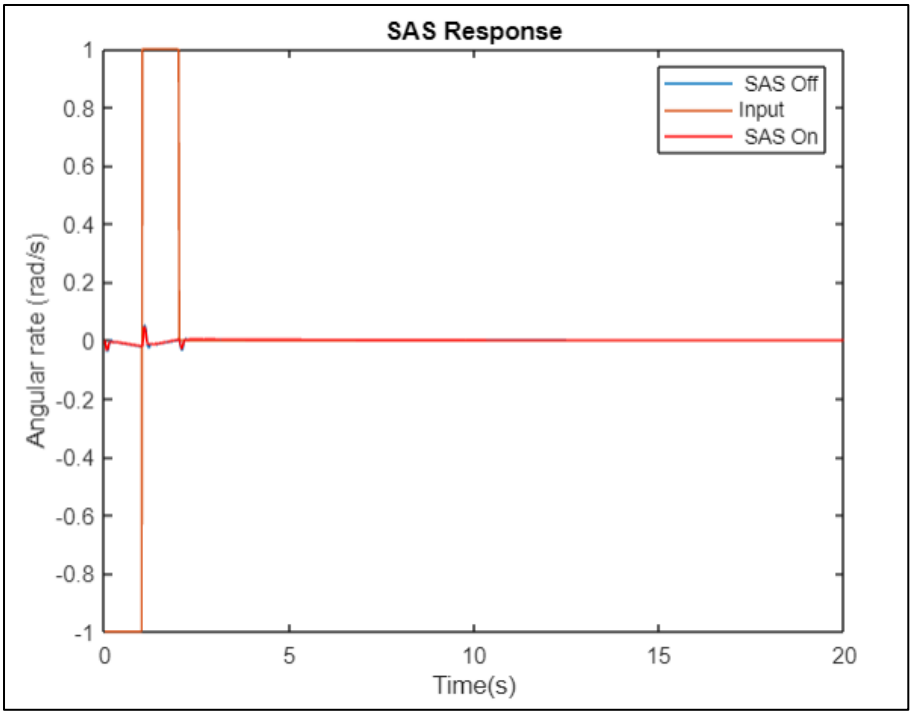

Figure 36: Stability Control System

Figure 36 illustrates the effects of the stability augmentation system (SAS) with a given input. It displays the output without the effects of the SAS in blue which shows minor but noticeable oscillations, in addition to the impact of the SAS where the oscillations are damped and converge in less time.

References

[1] "ABCGOODEFG 1000KV RC Brushless Motor A2212 13T with 30A Brushless ESC Set 1045 Propeller CW CCW Accessories Kit Mount for RC Plane Dji F450 550 Quadcopter, Electric Motors & Parts - Amazon Canada." *abcGoodefg 1000KV RC Brushless Motor A2212 13T with 30A Brushless ESC Set 1045 Propeller CW CCW Accessories Kit Mount for RC Plane DJI F450 550 Quadcopter, Electric Motors & Parts - Amazon Canada*, www.amazon.ca/abcGoodefg-Brushless-Propeller-Accessories-Quadcopter/dp/B08DXYLFQQ. Accessed 24 Mar. 2025.

[2] *Amazon.Com: Blomiky 2 Pack 11.1V 1500mAh 35C Lipo Battery with Deans T Plug for RC Airplane, RC Helicopter, RC Car Truck, RC Boat and Quadcopter Drone 11.1V 1500mah t 2 : Toys & Games*, www.amazon.com/Blomiky-Dean-Style-Airplane-Helicopter-Quadcopter/dp/B07DNZ16BV. Accessed 24 Mar. 2025.

[3] *Amazon.Com: Dafurui 10PCS SG90 Servo Motor, SG90 Mini 9G Micro ...*, www.amazon.com/DaFuRui-10PCS-Motor, -Arduino-Helicopter/dp/B0CDGZ6CG6. Accessed 24 Mar. 2025.

[4] Nelson, R.C. (2010) *Flight stability and automatic control*. Chennai: McGraw-Hill Education (India) Private Limited.

[5] Sadraey, M. H., *Aircraft design: A systems engineering approach*, Hoboken: Wiley, 2025.

[6] 2Campbell, J. P., and McKinney, M. O., "SUMMARY OF METHODS FOR CALCULATING DYNAMIC LATERAL STABILITY AND RESPONSE AND FOR ESTIMATING LATERAL STABILITY DERIVATIVES," *NATIONAL ADVISORY COMMITTEE FOR AERONAUTICS TECHNICAL NOTE 2409*, Jul. 1951.

[7] Stone, R. W., "ESTIMATION OF THE MAXIMUM ANGLE OF SIDESLIP FOR DETERMINATION OF VERTICAL-TAIL LOADS IN ROLLING MANEUVERS," *NATIONAL ADVISORY COMMITTEE FOR AERONAUTICS TECHNICAL NOTE 2633*, Feb. 1958.

Appendix A – Associated Code

Longitudinal Stability

```
% Estimating the Longtudinal Stability Derivatives Coefficients
% Mitchell Lacle
clc;clear all; close all;

% Initializing Parameters
M_project = 0.097;           % 33 (m/s) max flight speed at sea level
mass_full_scale = 0.938;     % Aircraft mass (kg)
g = 9.81;                    % Acceleration due to gravity (m/s^2)
rho = 1.225;                 % Air density at sea level (kg/m^3)
S_project = 0.335057;        % Wing area in m^2
b_project = 1.00919;         % Wingspan in meters
V_speed_flow = 340;          % Velocity of the airflow (m/s)
V_speed_project = 33;        % Aircraft max velocity (m/s)
V_cruise = 25;               % Velocity of the aircraft (m/s)
AR_w_project = 3.03968;      % Aspect ratio of wingspan relative to mean aerodynamic chord
AR_t_project = 1;            % Aspect ratio of the horizontal stab
S_F_project = 0.022;         % Horizontal tail surface area in m^2
lambda_project = 0.649;      % Taper Ratio
S_t = 0.0687;                % Wing area of the tail in m^2
d_F_project = 0.0506;        % Vertical tail length in meters
d_t = 0.44;                  % Distance of the tail in meters
Delta_w_project = 15.783;    % Change in downwash (in degrees)
z_w_project = 0.09989;       % Vertical location of the aerodynamic center in meters
d_project = 0.0925;          % Distance of the wings in meters
eta_project = 0.9;           % Efficiency Factor
e_project = 0.85;            % Oswald's Efficiency Factor
c_bar = 0.192;               % Mean aerodynamic chord (MAC) in meters
l_t = 0.424;                 % Tail moment arm in meters
d_epsilon_d_alpha = 0.3;     % Change in epsilon with respect to alpha
d_Cm_d_M = -0.289;
mu = 1.789e-5;               % Viscosity (Pa*s)
```

Lift Slope of Wing

```
Re = (rho * V_speed_project * c_bar) / mu;      % Reynolds number to get airfoil coefficient
values from airfoil tools
C_l_alpha = 0.11 * (180/pi);                    % 2D airfoil slope per radian
C_L_alpha2 = C_l_alpha / (1 + ...
    ((C_l_alpha)/(pi*e_project*AR_w_project))); % 3D estimated lift slope (per radian)
alpha_0 = 0;                                    % AoA of zero
alpha_L_at_0 = -3.8 * (pi/180);                 % Lift at zero AoA

C_L_0 = C_L_alpha2 * (alpha_0 - alpha_L_at_0);  % Estimated lift coefficient at AoA of zero
```

Slope of Horizontal Stabilizer

```
V_H = l_t * (S_t / (S_project * c_bar));          % Tail to wing moment arm ratio

alpha_L_at_0_t = 0;                               % AoA where lift = 0, since symmetric AoA = 0
C_l_alpha_t = 0.16 * (180/pi);                    % 2D lift slope of NACA 0009 at Re 50000
C_L_alpha_t = C_l_alpha_t / (1 + ...
    ((C_l_alpha_t)/(pi*e_project*AR_t_project))); % 3D lift slope of NACA 0009

C_L_0_t = C_L_alpha2 * (alpha_0 - alpha_L_at_0_t); % 3D lift coefficient of tail at zero AoA
```

Assumptions

```
C_T_u = -0.03;                  % due to variable pitch propeller flight
C_D_0 = 0.03;                   % thrust coefficient (due to variable pitch propeller flight)
C_d = 0.2;                      % base drag coefficient (estimated)
M = M_project;
D = 0.5 * rho * V_speed_project^2 .* C_d .* S_project;
Delta = 0;                      % sweep angle in terms of the rudder
d_C_d_d_M = (2 * D) / (rho * S_project * V_speed_project^2); % drag force
C_D_u = M_project * d_C_d_d_M;  % final drag coefficient calculation

% Lift Coefficient
W_full_scale = mass_full_scale * g;
C_L_project = W_full_scale / (0.5 * rho * V_cruise^2 * S_project);
```

Neutral Point and Downwash Angle

```
h_n_wb = 0.25;
K_n = 0.15;                                             % Static Margin
h_n = h_n_wb + (1/C_L_alpha2) * ( V_H * C_L_alpha_t);   % Neutral Point
h = h_n - K_n;                                          % CG

epsilon_0 = (2 * C_L_0) / (pi*AR_w_project);            % Downwash angle at zero AoA (Eq. 2.21 in
book)
```

X-Force Coefficient Derivatives

```
C_X_u = - (C_D_u + 2 * C_D_0) + C_T_u;

% X - direction coefficient due to the change of AoA
C_X_alpha = C_L_0 - (2*C_L_0 / (pi*e_project)) * (C_L_alpha2 / AR_w_project);

% X - direction coefficient due to the rate of change of AoA
C_X_alpha_dot = 0;

% X - direction coefficient due to pitching velocity
C_X_q = 0;
```

Z-Force Coefficient Derivatives

```
C_Z_u = - (M_project^2 / (1 - M_project^2)) * C_L_0 - 2 * C_L_0;

% Vertical force coefficient derivative with respect to AoA
C_Z_alpha = - (C_L_alpha2 + C_D_0);

% Vertical force coefficient derivative with respect to the rate of change of AoA
C_Z_alpha_dot = - 2 * V_H * eta_project * C_L_alpha_t * d_epsilon_d_alpha;

% Vertical force coefficient derivative with respect to pitch rate
C_Z_q = -2 * eta_project * C_L_alpha_t * V_H;
```

Pitching Moment Coefficient Derivatives

```
C_m_ac_wb = 0;        % Place holder for Exp / CFD results (Wing body nacelle pitching moment)
C_m_0_p = 0;          % Place holder for Exp / CFD results (Propulsive system pitching moment)

% Pitching moment coefficient derivative with respect to velocity
C_m_u = M_project * d_Cm_d_M;

% Pitching moment coefficient derivative with respect to AoA
```

```
C_m_alpha = C_L_alpha2 * (h - h_n_wb)  - C_L_alpha_t * V_H * (1 - d_epsilon_d_alpha);

% Pitching moment coefficient derivative with respect to the rate of change of AoA
C_m_alpha_dot = - 2 * V_H * eta_project * C_L_alpha_t * (l_t / c_bar) * d_epsilon_d_alpha;

% Pitching moment derivative with respect to pitch rate
C_m_q = - 2 * V_H * eta_project * C_L_alpha_t * (l_t / c_bar);

% Pitching moment coefficient at zero angle of attack
C_m_0 = C_m_ac_wb + C_m_0_p + C_L_alpha_t * V_H * (epsilon_0) * ( 1 - (S_t / S_project) ...
         * (C_L_alpha_t / C_L_alpha2) ...
         * (1 - d_epsilon_d_alpha));  % Neglecting the wing-body nacelle and propulsive system
pitching moments
```

Longitudinal Stability Coefficients

```
fprintf('<strong>X-Force Derivatives</strong>\n')
fprintf('C_X_u = %.4f\n',C_X_u)
fprintf('C_X_alpha = %.4f\n',C_X_alpha)
fprintf('C_X_alpha_dot = %.4f\n',C_X_alpha_dot)
fprintf('C_X_q = %.4f\n',C_X_q)


fprintf('<strong>Z-Force Derivatives</strong>\n')
fprintf('C_Z_u = %.4f\n',C_Z_u)
fprintf('C_Z_alpha = %.4f\n',C_Z_alpha)
fprintf('C_Z_alpha_dot = %.4f\n',C_Z_alpha_dot)
fprintf('C_Z_q = %.4f\n',C_Z_q)

fprintf('<strong>Pitching Moment Derivatives</strong>\n')
fprintf('C_m_u = %.4f\n',C_m_u)
fprintf('C_m_alpha = %.4f\n',C_m_alpha)
fprintf('C_m_alpha_dot = %.4f\n',C_m_alpha_dot)
fprintf('C_m_q = %.4f\n',C_m_q)
fprintf('C_m_0 = %.4f\n',C_m_0)
```

X-Force Derivatives

$C_{X_u} = -0.1094$

$C_{X_\alpha} = 0.0296$

$C_{X_{\dot{\alpha}}} = 0.0000$

$C_{X_q} = 0.0000$

Z-Force Derivatives

$C_{Z_u} = -0.4728$

$C_{Z_\alpha} = -3.5778$

$C_{Z_{\dot{\alpha}}} = -0.5056$

$C_{Z_q} = -1.6855$

Pitching Moment Derivatives

$C_{m_u} = -0.0280$

$C_{m_\alpha} = -0.2513$

$C_{m_{\dot{\alpha}}} = -1.1166$

$C_{m_q} = -3.7221$

$C_{m_0} = 0.0423$

Lateral Stability

Initial Values and Conditions

```
clc
clear all
close all

rho = 1.225; %kg/m^3
S = 0.335057; % Wing area in m^2
V = 33; %V_max m/s
l_t = 0.44; % Tail moment arm in meters
S_t = 0.0687; %vertical tail area m^2
c_bar = 0.192; %MAC
V_v = (S_t*l_t)/(S*c_bar) %Vertical fin volume ratio
d_sig_d_beta = 0.5; %Sidewash gradient
tail_eff = 0.8; %Tail efficiency factor

v_stall = 3.878; %Based upon milestone 1 (m/s)
v_max = 33; %Based upon milestone 1 (m/s)
sos_sl = 340; %Speed of sound at sea level (m/s)

C_n_Beta = 0.05:0.01:0.4; %Typical range for commercial aircraft (University of Sevilla)

AOA_F = deg2rad(-5:1:5); %All conditions involving AOA_F arbitrarily set for five degrees
Beta = deg2rad(0:3); %Typical fluxuation of sidewash angle (NACA)

a_f = deg2rad(0.02) %Lift-slope of vertical fin
a_r = deg2rad(2*pi); %lift-slope of rudder

delta_r = deg2rad([-24:1:24]); % Rudder deflection angle (University of Sevilla)
```

Lift-slope, Lift, and Moment for Vertical Tail

```
Cl_f = zeros(length(delta_r), length(AOA_F)); %Using the range for all the rudder deflection angles for
all values of AOA_f
for i = 1:length(AOA_F)
Cl_f(:, i) = a_f * AOA_F(i) + a_r * delta_r;
end

%Assuming AOA_f of 5 deg and rudder deflection angle of 24 deg
L_f = 0.5*rho*V^2 * S_t * max(Cl_f(:,11)) % N
N_f = -0.5*rho*V^2 * S_t * max(Cl_f(:,11)) * l_t %N-m
```

Yawing Moment and Weathercock Stability Contribution

```
Cn_f = -V_v * max(Cl_f(:,11)) %Assuming difference in relative airspeed for fuselage and vertical tail's
is negligible

d_Cn_f_d_beta = V_v*a_f*tail_eff*d_sig_d_beta %Contribution to weathercock stability
```

Roll Contributions

```
phi = deg2rad(0:1:25); %Roll angle
alpha_x = deg2rad(5); %AOA in X-direction
```

```
V_sideslip = v_max*sin(alpha_x)*sin(phi);

Beta_L9 = asin(V_sideslip/v_max);
max(rad2deg(Beta_L9))

Cl_beta = -0.4; %Dihedral effect

delta_cl = Cl_beta*alpha_x*max(phi)

Cl_phi = Cl_beta*alpha_x %roll stiffness
```

Lateral Dynamic Stability

```
A = [Xu Xw 0 -g; Zu Zw u0 0; Mu+(Mwdot*Zu) Mw+(Mwdot*Zw) Mq+(Mwdot*u0) 0; 0 0 1 0];
B = [XDeltae; ZDeltae; MDeltae + Mwdot*ZDeltae; 0]

fprintf(1,'2.) Results and Answer:\n');
[eigvec, eigval] = eig(A)

speigvec = eigvec(:,1);
speigvec(1,1) = speigvec(1,1)/u0;
speigvec(2,1) = speigvec(2,1)/u0;
speigvec(3,1) = speigvec(3,1)*c/(2*u0);

speigvec(1,1) = speigvec(1,1)/speigvec(4,1);
speigvec(2,1) = speigvec(2,1)/speigvec(4,1);
speigvec(3,1) = speigvec(3,1)/speigvec(4,1);
speigvec(4,1) = speigvec(4,1)/speigvec(4,1);

speigvec

lpeigvec = eigvec(:,4);

lpeigvec(1,1) = lpeigvec(1,1)/u0;
lpeigvec(2,1) = lpeigvec(2,1)/u0;
lpeigvec(3,1) = lpeigvec(3,1)*c/(2*u0);

lpeigvec(1,1) = lpeigvec(1,1)/lpeigvec(4,1);
lpeigvec(2,1) = lpeigvec(2,1)/lpeigvec(4,1);
lpeigvec(3,1) = lpeigvec(3,1)/lpeigvec(4,1);
lpeigvec(4,1) = lpeigvec(4,1)/lpeigvec(4,1);

lpeigvec

[eigvec, eigval] = eig(A);
eig_vals = diag(eigval);

eig_vals = diag(eigval2);

[~, eig_sort] = sort(real(eig_vals)); % sort by real part
eig_vals = eig_vals(eig_sort);

fprintf(1,'4.) Answers and Results:\n');

for i = 1:length(eig_vals)
if imag(eig_vals(i)) ~= 0
wn = abs(eig_vals(i)); % natural frequency
zeta = -real(eig_vals(i))/wn; % damping ratio
```

```
T = 2*pi/imag(eig_vals(i)); % period (if oscillatory)
fprintf('Dutch roll: Wn = %.2f rad/s, Damping = %.2f, Period = %.2f s\n', wn, zeta, T);
eig_vals(i)
wd = (2*pi)/T
else
if abs(eig_vals(i)) < 1
fprintf('Spiral mode: Eigenvalue = %.4f\n', eig_vals(i));
time_con = 1/abs(eig_vals(i))
else
fprintf('Roll convergence mode: Eigenvalue = %.4f\n', eig_vals(i));
time_con = 1/abs(eig_vals(i))
end
end
end

x0 = [0; 0; 0; 1];

sys = ss(A_2, zeros(4,1), eye(4), zeros(4,1));
t = linspace(0, 20, 1000); % simulate for 20 seconds
[y, t, x] = initial(sys, x0, t);
figure
hold on
plot(t, x(:,1))
xlabel('Time (s)')
ylabel('Sideslip Angle (rad)')
title('Response of Sideslip Angle to Unit Impulse in Roll Angle ')
grid on
hold off
```

Longitudinal Dynamic Stability

```
for C_n_beta_wf = 0:0.01:1

% From L13-8
% Eqn. for C_n_beta from Lecture 12-9
C_n_beta = C_n_beta_wf + V_v_p*C_L_alpha_v_p*vTail_eta_and_dsig_dBeta;

Y_beta = q*S_project*C_y_beta_p/mass_full_scale;
Y_p = q*S_project*b_project*C_y_p/(2*mass_full_scale*V_cruise);
Y_r = q*S_project*b_project*C_y_r/(2*mass_full_scale*V_cruise);

L_beta = q*S_project*b_project*C_l_beta/Ix_p;
L_p = q*S_project*b_project^2*C_l_p/(2*Ix_p*V_cruise);
L_r = q*S_project*b_project^2*C_l_r/(2*Ix_p*V_cruise);

N_beta = q*S_project*b_project*C_n_beta/Iz_p;
N_p = q*S_project*b_project^2*C_n_p/(2*Iz_p*V_cruise);
N_r = q*S_project*b_project^2*C_n_r/(2*Iz_p*V_cruise);

Y_delta_r = q*S_project*b_project*C_y_r/(2*mass_full_scale*V_cruise);
L_delta_a = q*S_project*b_project*C_l_delta_a/Ix_p;
L_delta_r = q*S_project*b_project*C_l_delta_r/Ix_p;
N_delta_a = q*S_project*b_project*C_n_delta_a/Iz_p;
N_delta_r = q*S_project*b_project*C_n_delta_r/Iz_p;

A_2 = [Y_beta/V_cruise Y_p/V_cruise -(1-Y_r/V_cruise) g*cos(theta)/V_cruise;
L_beta L_p L_r 0 ;
N_beta N_p N_r 0;
0 1 0 0];
```

```
B_2 = [ 0 Y_delta_r/V_cruise;
L_delta_a L_delta_r;
N_delta_a N_delta_r;
0 0 ];
V2 = [B_2 A_2*B_2 A_2^2*B_2 A_2^3*B_2];
rank(V2); % this is 4, so the aircraft is controllable using rudder and aileron

[eigvec2, eigval2] = eig(A_2);

real12(ind2)=real(eigval2(1,1));
Img12(ind2)=imag(eigval2(1,1));
real22(ind2)=real(eigval2(2,2));
Img22(ind2)=imag(eigval2(2,2));
real32(ind2)=real(eigval2(3,3));
Img32(ind2)=imag(eigval2(3,3));
real42(ind2)=real(eigval2(4,4));
Img42(ind2)=imag(eigval2(4,4));
ind2=ind2+1;
end

fprintf(1,'3.) Answers and Results:\n');

for i = 1:length(eig_vals)
if imag(eig_vals(i)) ~= 0
wn = abs(eig_vals(i)); % natural frequency
zeta = -real(eig_vals(i))/wn; % damping ratio
T = 2*pi/imag(eig_vals(i)); % period
fprintf('Phugoid : Wn = %.2f rad/s, Damping = %.2f, Period = %.2f s\n', wn, zeta, T);
else
fprintf('Short period = %.4f \n', eig_vals(i));
wn = abs(eig_vals(i)); % natural frequency
zeta = -real(eig_vals(i))/wn; % damping ratio
T = 2*pi/imag(eig_vals(i)); % period
fprintf('Short period : Wn = %.2f rad/s, Damping = %.2f, Period = %.2f s\n', wn, zeta, T);
end
end

x0 = [1; 0; 0; 0]; % Unit impulse in speed u

sys = ss(A, zeros(4,1), eye(4), zeros(4,1));
t = linspace(0, 20, 1000); % simulate for 20 seconds
[y, t, x] = initial(sys, x0, t);

figure;
plot(t, x(:,2)); % w is index 2
xlabel('Time (s)');
ylabel('Angle of Attack (rads)');
title('Response of AoA to Unit Impulse in Speed');
```

Root Locus filtering out AoA

```
temp = [0 0 0 0 0];
A2 = [A1';temp]';
A2 = [A2; 0 1/(tauF*u0) 0 0 0 -1/tauF]

B2 = [B1; 0];
%C2 = [0 1/u0 0 0 0 0]; % for want AoA
C2 = [0 0 0 0 0 1]; % for want filtered AoA
```

```
figure(2);
hold on
rlocus(A2,B2,C2,0,kalpha);
grid on;
hold off
```

Impulse Response

```
clear kalpha
kalpha = 5; % pick a gain
C2prime = [0 0 0 0 0 1];
figure(1);
title(' Impulse response');
xlabel(' Time (s)');
A3 = A2 + B2*C2prime*kalpha;
[b,a] = ss2tf(A3,B2,[0 1/u0 0 0 0 0],0);
hold on;
[imp_res, tim]=impulse(tf(b,a)); % compare impulse responses
%step(tf(b,a))
plot(tim, imp_res,'g--','linewidth',2)
legend('Open Loop', 'Close Loop SAS');
ylabel(' Angle of Attack (rad)');
hold off
```

Step Response

```
figure(3)
hold on
grid on
[step_res, step_tim] = step(tf(b,a))

plot(step_tim, step_res,'g--')
title('Step Response')
ylabel('Angle of attack (Rad)')
xlabel('Time')
hold off
```

Stability Augmentation System

```
V = [B_2 A_2*B_2 A_2^2*B_2 A_2^3*B_2];
rank(V)
[eigvec eigval] = eig(A_2)
C = [0 1 0 0; 0 0 1 0]; % we are interested in roll rate and yaw rate
D = [0 0; 0 0];
plant = ss(A_2,B_2,C,D); % define plant
% define actuator
aa = [-10 0; 0 -20] ;
ba = [1 0; 0 1];
ca = [-0.1 0; 0 -0.1]; % phase reversal of actuator, positive control displacementyields negative
moments
da = [0 0; 0 0];
actu = ss(aa,ba,ca,da);
% end define actuator
sys1 = series(actu,plant); % Combine the transfer functions
[a,b,c,d] = ssdata(sys1);
k = 0:0.1:100;
figure(4);
rlocus(a,b(:,1),c(1,:),0,k) % rootlocus on roll rate feedback
```

```
 %plot(rootlocusplotroll);
 kp = 0.01;
 acl1 = a - b(:,1)*kp*c(1,:); % closed loop roll
 figure(5);
 rlocus(acl1,b(:,2),c(2,:),0,k) % rootlocus on yaw rate feedback
 kr = 5;
 % acl2 = a-b*[kp 0;
 %
 acl2 = a - b*[kp 0;0 kr]*c; % closed loop system matrix after closing both loops
 t = [0:0.02:20];
 u = [-ones(1,51), ones(1,50), zeros(1,900)];
 figure(6);
 [y,x]=lsim(a,b(:,2),c(2,:),0,u,t); % response of OLTF to aileron/rudder doublet, change b and c colums
to go from each input to either output
 plot(t,y,t,u);
 hold on;
 [y1,x1]=lsim(acl2,b(:,2),c(2,:),0,u,t); % response of CLTF to aileron/rudder doublet, change b and c
colums to go from each input to either output
 plot(t,y1,'r');
 legend(' SAS Off', 'Input',' SAS On');
```